ARTICLE

https://doi.org/10.1038/s41586-019-1503-x

BCAA catabolism in brown fat controls energy homeostasis through SLC25A44

Takeshi Yoneshiro[1,2,3,14], Qiang Wang[1,2,3,14], Kazuki Tajima[1,2,3], Mami Matsushita[4], Hiroko Maki[5], Kaori Igarashi[5], Zhipeng Dai[6], Phillip J. White[7], Robert W. McGarrah[7], Olga R. Ilkayeva[7], Yann Deleye[7], Yasuo Oguri[1,2,3], Mito Kuroda[1,2,3], Kenji Ikeda[1,2,3,8], Huixia Li[1,2,3], Ayano Ueno[5], Maki Ohishi[5], Takamasa Ishikawa[5], Kyeongkyu Kim[1,2,3], Yong Chen[1,2,3], Carlos Henrique Sponton[1,2,3], Rachana N. Pradhan[1,2,3], Homa Majd[2], Vanille Juliette Greiner[1,9], Momoko Yoneshiro[1,2,3], Zachary Brown[1,2,3], Maria Chondronikola[10], Haruya Takahashi[11], Tsuyoshi Goto[11], Teruo Kawada[11], Labros Sidossis[12], Francis C. Szoka[6], Michael T. McManus[1,9], Masayuki Saito[13], Tomoyoshi Soga[5] & Shingo Kajimura[1,2,3]*

Branched-chain amino acid (BCAA; valine, leucine and isoleucine) supplementation is often beneficial to energy expenditure; however, increased circulating levels of BCAA are linked to obesity and diabetes. The mechanisms of this paradox remain unclear. Here we report that, on cold exposure, brown adipose tissue (BAT) actively utilizes BCAA in the mitochondria for thermogenesis and promotes systemic BCAA clearance in mice and humans. In turn, a BAT-specific defect in BCAA catabolism attenuates systemic BCAA clearance, BAT fuel oxidation and thermogenesis, leading to diet-induced obesity and glucose intolerance. Mechanistically, active BCAA catabolism in BAT is mediated by SLC25A44, which transports BCAAs into mitochondria. Our results suggest that BAT serves as a key metabolic filter that controls BCAA clearance via SLC25A44, thereby contributing to the improvement of metabolic health.

In addition to the well-known function of BAT as a thermogenic organ, studies using positron emission tomography–computed tomography (PET–CT) with ^{18}F-fluorodeoxyglucose (^{18}F-FDG) and fatty-acid tracers have demonstrated that BAT also serves as a metabolic sink for glucose and fatty acids[1–3]. This function is tightly coupled with the ability to improve metabolic health: cold acclimatization stimulates uptake of glucose, triglyceride-rich lipoproteins and fatty acids in BAT, thereby contributing to improved systemic lipid metabolism[4,5]. It remains unknown, however, whether BAT contributes to the clearance of any other metabolites and how such processes are regulated. Accordingly, we performed an unbiased metabolite analysis on sera from healthy human subjects (male, aged 23.4 ± 0.6 years old (all results are shown as mean ± s.e.m.), $n = 33$) with high BAT activity (standardized uptake value (SUV) > 4.03, $n = 17$) and low BAT activity (SUV ≤ 4.03, $n = 16$) at 27 °C (thermoneutral) and following cold exposure (19 °C) for 2 h (Supplementary Table1). Subjects with SUV > 4.03 were considered as the high-BAT group, on the basis of the median of the subjects in the study (Fig. 1a). The cold stimulus of 19 °C was selected on the basis that BAT thermogenesis is stimulated at 19 °C in adults without triggering skeletal muscle shivering (Extended Data Fig. 1a). Cold exposure stimulated lipolysis in adipose tissue, leading to a significant increase in circulating levels of non-esterified fatty acids in both groups, whereas cold exposure did not change blood glucose levels (Extended Data Fig. 1b, c).

Cold-activated BAT promotes systemic BCAA clearance

Unexpectedly, we found that serum concentration of Val was significantly reduced, preferentially in high-BAT subjects following cold exposure, whereas no significant change was seen in low-BAT subjects (Fig. 1b). The cold-induced reduction in serum Val concentrations showed a significant inverse correlation with BAT activity measured by ^{18}F-FDG-PET imaging (Fig. 1c). Similarly, cold-induced changes in Leu and total BCAA levels were inversely correlated with SUV, whereas no amino acids except Val and Leu showed a significant correlation (Fig. 1d, Extended Data Fig. 1d, Supplementary Table 2). Although skeletal muscle is a major organ that utilizes BCAA, there was no correlation of muscle mass with cold-induced changes in BCAA levels (Extended Data Fig. 1e). Consistent with the human study, plasma metabolomics in obese mice showed that cold exposure significantly reduced plasma Val, Leu and Ile levels (Fig. 1e, Extended Data Fig. 1f).

These observations caught our attention because epidemiological studies have demonstrated that increased circulating BCAA levels are strongly associated with obesity, insulin resistance and type 2 diabetes in humans and rodents[6–8], despite the fact that BCAA supplementation in healthy subjects is often associated with beneficial effects on muscle growth and energy expenditure[9]. Expression or activity of mitochondrial BCAA enzymes, such as the branched-chain α-keto acid dehydrogenase (BCKDH) complex, in the white adipose tissue (WAT) is reduced in obese and diabetic states[10–13], and transplantation of WAT from wild-type mice into branched-chain aminotransferase (BCAT2)-deficient mice reduces circulating BCAA levels[13], suggesting that adipose tissue contributes to the regulation of circulating BCAA levels. The extent to which cold acclimatization controls systemic BCAA homeostasis via BAT remains unknown.

Thus, we visualized Leu uptake in BAT using a PET–CT scan with ^{18}F-fluciclovine, a Leu-analogue tracer. Following cold acclimatization, ^{18}F-fluciclovine-PET–CT detected a robust increase in ^{18}F-fluciclovine uptake in the BAT and a modest increase in the inguinal WAT of mice

[1]UCSF Diabetes Center, San Francisco, CA, USA. [2]Eli and Edythe Broad Center of Regeneration Medicine and Stem Cell Research, San Francisco, CA, USA. [3]Department of Cell and Tissue Biology, University of California, San Francisco, San Francisco, CA, USA. [4]Department of Nutrition, Tenshi College, Sapporo, Japan. [5]Institute for Advanced Biosciences, Keio University, Yamagata, Japan. [6]Department of Bioengineering and Therapeutic Sciences, University of California, San Francisco, San Francisco, CA, USA. [7]Duke Molecular Physiology Institute, Duke University, Durham, NC, USA. [8]Department of Molecular Endocrinology and Metabolism, Tokyo Medical and Dental University, Tokyo, Japan. [9]Department of Microbiology and Immunology, University of California, San Francisco, San Francisco, CA, USA. [10]Center for Human Nutrition, Washington University in St Louis, St Louis, MO, USA. [11]Laboratory of Molecular Function of Food, Graduate School of Agriculture, Kyoto University, Uji, Japan. [12]Department of Kinesiology and Health, School of Arts and Sciences, Rutgers University, New Brunswick, NJ, USA. [13]Department of Biomedical Sciences, Graduate School of Veterinary Medicine, Hokkaido University, Sapporo, Japan. [14]These authors contributed equally: Takeshi Yoneshiro, Qiang Wang. *e-mail: shingo.kajimura@ucsf.edu

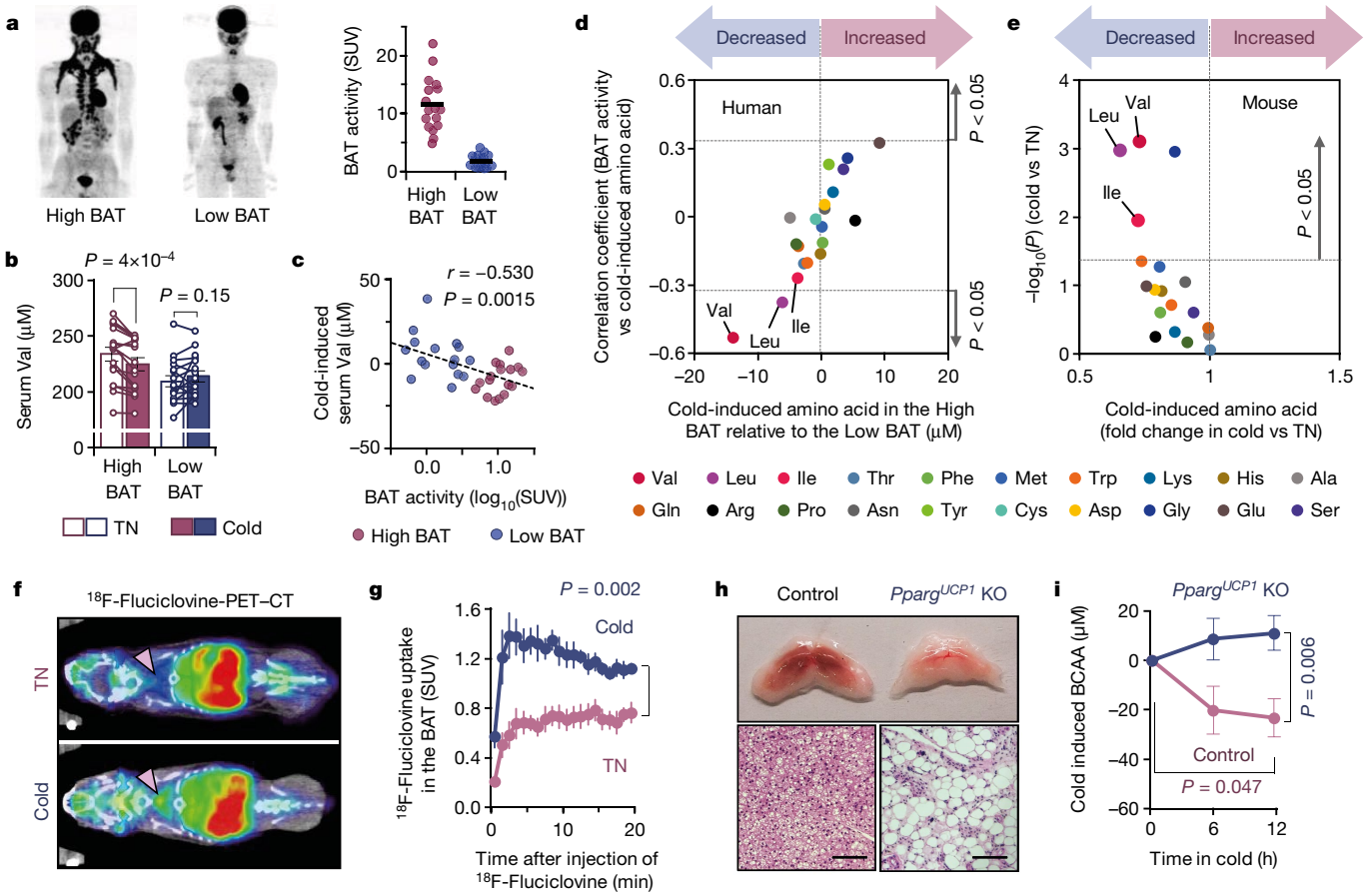

Fig. 1 | Cold-induced BAT thermogenesis promotes systemic BCAA clearance in mice and humans. a, Left, ^{18}F-FDG-PET–CT images of human experimental subjects following cold exposure. Right, SUV of ^{18}F-FDG in the BAT deposits. $n = 17$ (high BAT), $n = 16$ (low BAT). **b**, Circulating Val concentration in subjects in **a** at 27 °C (thermoneutral) and at 19 °C (cold). **c**, Correlation between BAT activity and cold-induced changes in serum Val concentration in **a**. **d**, Correlation between cold-induced amino acid changes and BAT activity (*y* axis) against the degree of BAT-dependent amino acid changes (*x* axis) in **a**. **e**, Cold-induced changes in plasma amino acids in diet-induced obese mice at 30 °C (thermoneutral (TN), $n = 5$) or 15 °C (cold, $n = 6$). **f**, ^{18}F-Fluciclovine-PET–CT images of mice acclimatized to 30 °C (TN) or 15 °C (cold) for two weeks. Arrows indicate interscapular BAT. **g**, SUV of ^{18}F-fluciclovine in BAT. $n = 5$ per group. **h**, Morphology and haematoxylin and eosin (H&E) staining of interscapular BAT of *Pparg*^{UCP1}-KO and control mice. Scale bars, 50 μm. Representative result from two independent experiments. **i**, Plasma levels of BCAA in **h** during cold temperature (12 °C). $n = 7$ per group. **a**–**i**, Biologically independent samples. Data are mean ± s.e.m.; two-sided *P* values by paired *t*-test (**b**), unpaired Student's *t*-test (**e**), or two-way repeated measures analysis of variance (ANOVA) (**g**) followed by post hoc paired or unpaired *t*-tests with Bonferroni's correction (**i**). Pearson's or Spearman's rank correlation coefficient was calculated, as appropriate (**c**, **d**).

(Fig. 1f, g). Whereas the basal SUV in the liver and heart was higher than in BAT, no significant change was seen in these organs following cold exposure (Extended Data Fig. 2a). Consistent with a recent study[14], we found that BAT displayed the highest Val oxidation on cold exposure, relative to other metabolic organs including inguinal WAT, epididymal WAT and gastrocnemius muscle of mice (Extended Data Fig. 2b, c). Furthermore, Val oxidation in differentiated human brown adipocytes was significantly higher than in white adipocytes and was further enhanced by noradrenaline (Extended Data Fig. 2d). Of note, transcriptomics and proteomics data from mice and humans[15–17] showed that more than 60% of genes encoding BCAA catabolic enzymes, including the gene for the rate-limiting enzyme BCAT2, were more highly expressed in brown adipocytes relative to white adipocytes (Extended Data Fig. 2e, f). Our previous analysis in humans[5] also found that the BCAA catabolic pathway was highly and selectively induced by cold exposure in the supraclavicular BAT but not in the abdominal WAT (Extended Data Fig. 2g). Notably, BCAA is oxidized primarily in the mitochondria of BAT; BAT predominantly expresses the mitochondria-localized form BCAT2, but not the cytosolic isoform BCAT1 (Extended Data Fig. 2h, i). Despite this knowledge, the mitochondrial transporter for BCAAs is unidentified, and it remains unknown how BCAAs are utilized in brown adipocytes.

To determine whether BAT contributes to systemic BCAA clearance, we generated a BAT-ablation mouse model in which peroxisome proliferator-activated receptor-γ (PPAR-γ) was deleted in uncoupling protein 1 (UCP1)-expressing thermogenic adipocytes (*Pparg*^{UCP1} knockout (KO), *Ucp1-cre*;*Pparg*$^{flox/flox}$). In contrast to littermate controls (*Pparg*$^{flox/flox}$), the presumptive BAT in *Pparg*^{UCP1}-KO mice was composed of unilocular adipocytes and fibrotic tissues (Fig. 1h). Following cold exposure, plasma BCAA concentration was significantly reduced in control mice but not in *Pparg*^{UCP1}-KO mice (Fig. 1i).

BAT-specific BCAA defect impairs energy homeostasis

To examine the extent to which BCAA catabolism in BAT regulates energy homeostasis, we next generated a mouse model in which BCAA oxidation is impaired specifically in the BAT (*Bckdha*^{UCP1}-KO mice, *Ucp1-cre*;*Bckdha*$^{flox/flox}$) (Fig. 2a, Extended Data Fig. 3a–c). Whereas no difference was seen in BAT mass and thermogenic gene expression between the genotypes on a regular diet (Extended Data Fig. 3d, e), the core-body temperature of *Bckdha*^{UCP1}-KO mice was significantly lower than that of controls after cold exposure without affecting muscle shivering (Fig. 2b, Extended Data Fig. 3f). Tissue-temperature recording also detected impaired thermogenesis in the BAT of *Bckdha*^{UCP1}-KO mice following treatment with noradrenaline, whereas no change was

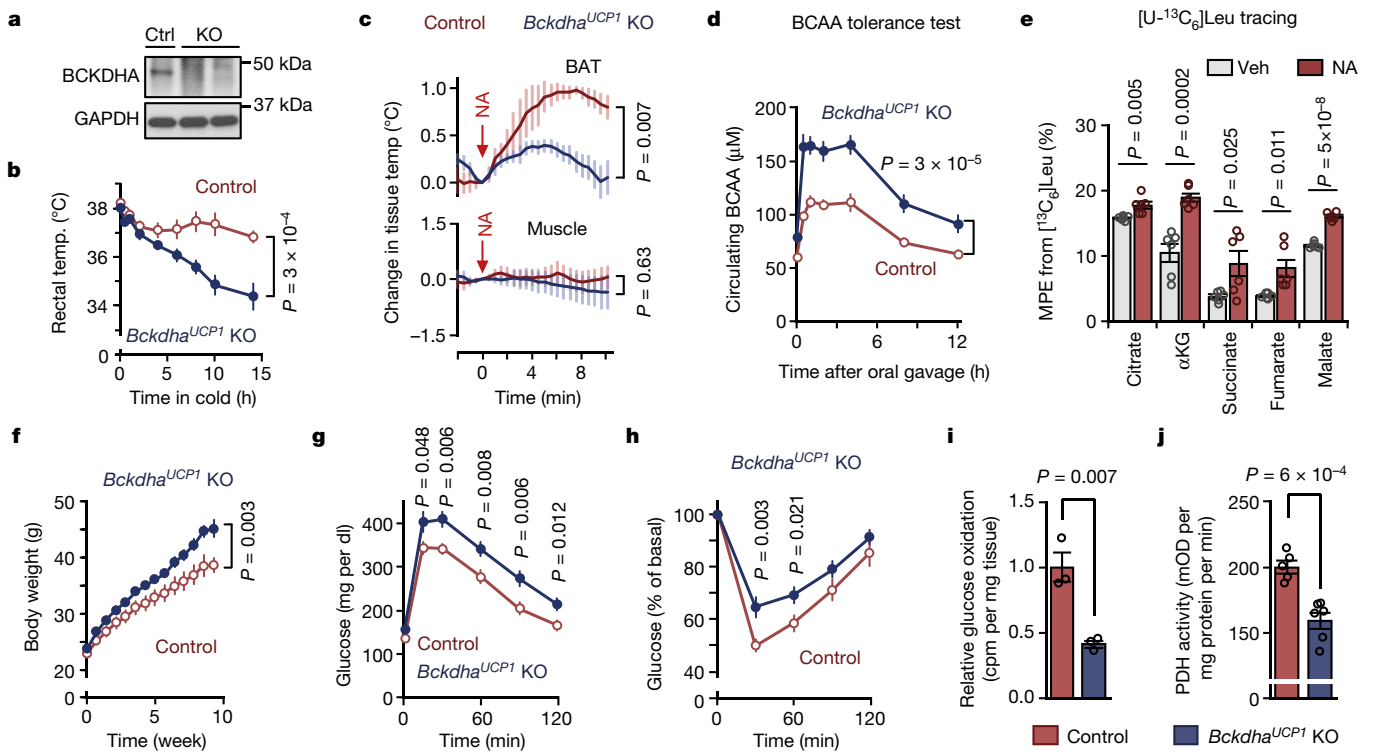

Fig. 2 | BCAA oxidation in BAT is required for BCAA clearance and energy homeostasis. a, Immunoblotting of BCKDHA in BAT of *Bckdha*^{UCP1}-KO and control (ctrl) mice. GAPDH was used as a loading control. Representative result from two independent experiments. Gel source data are presented in Supplementary Fig. 1. **b**, Rectal core body temperature following cold exposure at 8 °C. $n = 8$ (control), $n = 9$ (*Bckdha*^{UCP1}-KO). **c**, Change in tissue temperature (temp) in BAT and muscle following treatment with noradrenaline (NA). $n = 4$ per group. **d**, Plasma BCAA levels at indicated time points after a BCAA oral gavage at 12 °C. $n = 8$ per group. **e**, MPE of indicated metabolites derived from [U-^{13}C$_6$]Leu in human brown adipocytes. Cells were treated with vehicle (veh) or noradrenaline for 1 h. $n = 6$ per group. αKG, α-ketoglutarate. **f**, Body weight of *Bckdha*^{UCP1}-KO ($n = 15$) and control ($n = 13$) mice on high-fat diet at ambient temperature. **g**, Glucose tolerance test of mice in **f**. **h**, Insulin tolerance test of mice in **f**. **i**, Glucose oxidation in BAT normalized to tissue mass. $n = 3$ mice per group. **j**, PDH activity in BAT of mice maintained at 12 °C for one week. $n = 5$ (control), $n = 6$ (*Bckdha*^{UCP1}-KO). **b**–**j**, Biologically independent samples. Data are mean ± s.e.m.; two-sided *P* values by unpaired Student's *t*-test (**e**, **i**, **j**) or two-way repeated measures ANOVA (**b**–**d**, **f**) followed by post hoc unpaired *t*-test (**g**, **h**).

seen in muscle and liver temperature (Fig. 2c, Extended Data Fig. 3g). Notably, *Bckdha*^{UCP1}-KO mice were intolerant to oral BCAA challenge compared with control mice (Fig. 2d, Extended Data Fig. 3h). Similarly, *Bckdha*^{UCP1}-KO mice displayed higher plasma BCAA levels than controls following cold exposure (Extended Data Fig. 3i). These results indicate that BCAA oxidation is required for BAT thermogenesis and systemic BCAA clearance.

To examine how a cold stimulus alters BCAA utilization in brown fat, we next used capillary electrophoresis time-of-flight mass spectrometry (CE-TOFMS) and performed Leu stable-isotope tracing in differentiated human brown adipocytes. The mole percentage enrichment (MPE) of tricarboxylic acid (TCA) cycle intermediates derived from [U-^{13}C$_6$]Leu was quantified following noradrenaline treatment for 1 h (Extended Data Fig. 4a, Supplementary Table 3). We found that acute noradrenaline treatment significantly increased the MPE of TCA intermediates, including succinate (Fig. 2e, Extended Data Fig. 4b), although the fractional contribution of labelled Leu to the TCA cycle was relatively small. This rapid noradrenaline-stimulated BCAA oxidation was aligned with increased expression of many BCAA-oxidation enzymes in the BAT mitochondria within 8 h after cold exposure (Extended Data Fig. 4c, d) and the rapid oxidation of BCAA in BAT[14]. Of note, Val supplementation rapidly increased oxygen consumption rate (OCR) in human brown adipocytes stimulated with noradrenaline (Extended Data Fig. 4e). The stimulatory effect requires the generation of the TCA-cycle intermediate succinate: inhibition of succinyl coenzyme A synthetase or succinate dehydrogenase by vanadate or malonate, respectively, blunted the Val effect on OCR (Extended Data Fig. 4f, g). We also found that supplementation of Val, Leu or Ile significantly enhanced noradrenaline-stimulated thermogenesis in brown adipocytes in a UCP1-dependent fashion (Extended Data Fig. 4h, i). BCAA supplementation or pharmacological BCAT2 activation significantly increased brown fat respiration in a BCKDHA-dependent manner; the reduced respiration in *Bckdha*-deficient cells was not the result of a general mitochondrial defect, because succinate supplementation, but not α-ketoisovalerate (KIV), restored noradrenaline-stimulated thermogenesis in *Bckdha*-deficient brown adipocytes (Extended Data Fig. 4i, j). Previous studies report that BCAA catabolism fuels de novo lipogenesis by generating monomethyl branched-chain fatty acids (mmBCFAs), and that mmBCFA synthesis in BAT is activated after one month of cold acclimatization[18,19]. Consistent with these studies, proteomics data showed that the expression of mmBCFA synthesis enzymes, including carnitine acetyltransferase, were increased after three-week cold acclimatization, whereas many BCAA oxidative enzymes in the mitochondria were rapidly induced within 8 h of cold exposure and subsequently downregulated (Extended Data Fig. 4c, d). These data suggest a dynamic shift in BCAA utilization during cold acclimatization in BAT; that is, acute cold exposure activates BCAA oxidation in the TCA cycle, whereas chronic cold gradually promotes mmBCFA synthesis.

Next, we examined the degree to which a BAT-specific defect in BCAA catabolism influences whole-body metabolism. *Bckdha*^{UCP1}-KO mice on a high-fat diet gained significantly more body weight than littermate controls, owing to increased adipose tissue and liver mass, but not to changes in lean mass or food intake (Fig. 2f, Extended Data Fig. 5a–c). Consistent with previous studies showing that BAT thermogenesis controls hepatic triglyceride clearance[4,20], the livers

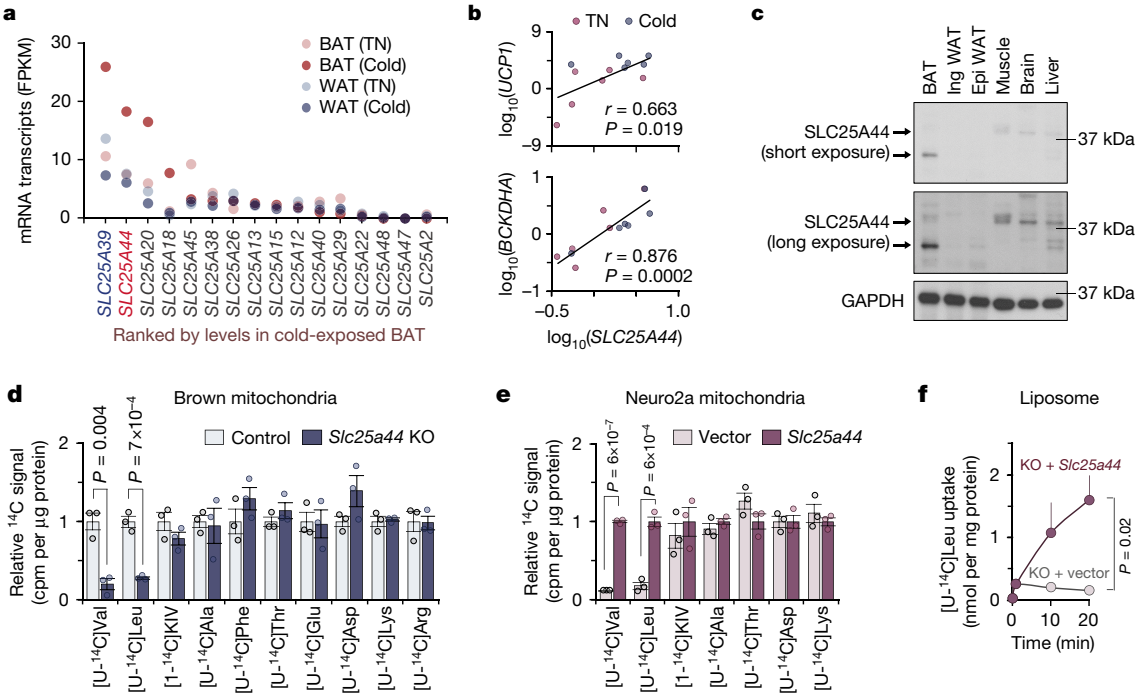

Fig. 3 | Identification of SLC25A44 as a mitochondrial BCAA transporter. **a**, Expression profile of SLC25A family members in human supraclavicular BAT and abdominal subcutaneous WAT from the same individual at 27 °C and 19 °C (ref. [5]). FPKM, fragments per kilobase of transcript per million mapped reads. **b**, Correlation of expression of *SLC25A44* mRNA with that of *UCP1* or *BCKDHA* in human BAT. Expression in thermoneutral (red) or cold (blue) conditions from six biologically independent subjects. *r*, Pearson's correlation coefficient. **c**, SLC25A44 protein expression in indicated tissues of mice. GAPDH was used as a loading control. Representative result from two independent experiments. Gel source data are presented in Supplementary Fig. 1. **d**, **e**, Mitochondrial uptake of indicated molecules in control and *Slc25a44*-KO brown adipocytes (**d**) or in Neuro2a cells expressing *Slc25a44* or an empty vector (**e**). $n = 3$ biologically independent samples per group. **f**, [U-$^{14}C_6$]Leu transport into mitochondrial liposomes from *Slc25a44*-KO brown adipocytes, expressing an empty vector (KO + vector) or *Slc25a44* (KO + *Slc25a44*). $n = 3$ technically independent samples per group. Representative result from two independent experiments. Data are mean ± s.e.m.; two-sided *P* values by unpaired Student's *t*-test (**d**, **e**) or two-way ANOVA (**f**).

of *Bckdha*^{UCP1} -KO mice contained significantly higher levels of triglycerides than those of controls (Extended Data Fig. 5d). Of note, *Bckdha*^{UCP1}-KO mice exhibited increased systemic glucose intolerance and insulin resistance compared with controls (Fig. 2g, h). Furthermore, glucose oxidation in the BAT of *Bckdha*^{UCP1}-KO mice was significantly reduced relative to controls (Fig. 2i). Fatty acid oxidation in the BAT of *Bckdha*^{UCP1}-KO mice was modestly reduced relative to controls (Extended Data Fig. 5e). The impaired glucose oxidation in *Bckdha*^{UCP1}-KO mice was associated with reduced pyruvate dehydrogenase (PDH) activity in the BAT and inguinal WAT, and with increased phosphorylation of the E1 subunit of PDH at S300 and, to a lesser degree, at S293 (Fig. 2j, Extended Data Fig. 5f–h).

SLC25A44 mediates mitochondrial BCAA transport

Recognizing the role of BCAA catabolism in BAT thermogenesis, we next sought to answer the long-standing question: how do cells take up BCAAs into the mitochondria? As described earlier, brown adipocytes in humans and mice predominantly express the mitochondria-localized isoform BCAT2 in preference to BCAT1, but the mitochondrial BCAA transporter remains uncharacterized. Therefore, we hypothesized that thermogenic adipocytes would express a mitochondrial BCAA transporter. Members of the SLC25A family are promising candidates for this role, because many of the mitochondrial amino acid transporters belong to this family of solute carrier transporter proteins[21]. In addition to the carnitine–acylcarnitine translocase SLC25A20 and the glutamate carrier SLC25A22, transcriptome analyses identified two uncharacterized SLC25A members, SLC25A39 and SLC25A44 that were abundantly expressed in mouse and human BAT (Fig. 3a, Extended Data Fig. 6a). Expression of *SLC25A44*, but not *SLC25A39* mRNA in the human supraclavicular BAT was significantly increased after cold exposure and showed a positive correlation with *UCP1* and *BCKDHA* mRNA expression (Fig. 3b, Extended Data Fig. 6b). SLC25A44 protein was localized to the mitochondria and more highly expressed in the BAT compared with other metabolic organs (Fig. 3c, Extended Data Fig. 6c, d). In addition, SLC25A44 expression was increased during brown adipogenesis (Extended Data Fig. 6e–g).

To determine the function of SLC25A44, we generated *Slc25a44*-KO brown adipocytes using CRISPR–Cas9 (Extended Data Fig. 7a). Mitochondrial BCAA uptake assays showed that Val and Leu uptake was selectively and significantly reduced in *Slc25a44*-KO cells, whereas *Slc25a44* deletion did not affect the mitochondrial uptake of other amino acids (Fig. 3d, Extended Data Fig. 7b, c). Similarly, depletion of *Slc25a44* by lentivirus short-hairpin RNAs (shRNAs) abrogated mitochondrial Val and Leu uptake, whereas *Slc25a39* depletion did not affect Val and Leu uptake (Extended Data Fig. 7d, e). Conversely, ectopic expression of SLC25A44 in a neuroblastoma cell line (Neuro2a cells) with undetectable endogenous SLC25A44 sufficiently and selectively restored mitochondrial Val and Leu uptake (Fig. 3e, Extended Data Fig. 7f).

To characterize SLC25A44 in a cell-free system, we prepared liposomes that were fused with the mitochondrial inner membrane from *Slc25a44*-KO brown adipocytes or *Slc25a44*-KO cells that ectopically expressed *Slc25a44* (Extended Data Fig. 7g, h). We observed robust and rapid Leu uptake in the mitochondrial liposomes from SLC25A44-expressing cells that were preloaded with Leu and Glu, whereas there was no detectable Leu uptake in the control group (Fig. 3f, Extended Data Fig. 7i). There was no difference in Glu uptake between the two groups (Extended Data Fig. 7j). As an alternative cell-free system, we reconstituted proteoliposomes by fusing liposomes with purified SLC25A44 protein (Extended Data Fig. 7k, l). Consistent with the results from mitochondrial liposomes, we detected active Leu uptake into the proteoliposomes with purified SLC25A44 (Extended Data Fig. 7m).

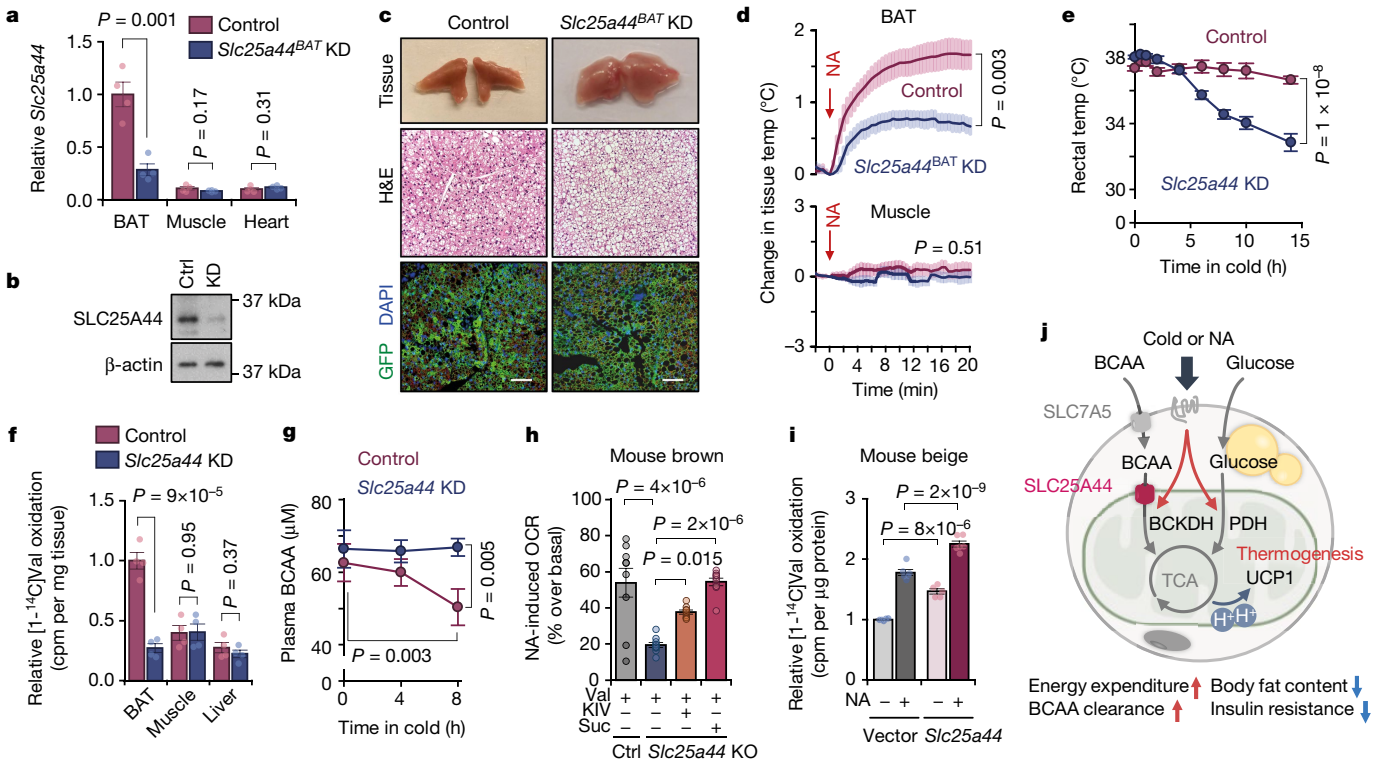

Fig. 4 | SLC25A44 is required for BAT thermogenesis and BCAA catabolism. **a**, Expression of *Slc25a44* mRNA in indicated tissues of *Slc25a44*^{BAT}-KD and control mice. $n = 4$ per group. **b**, Immunoblotting of SLC25A44 in BAT of mice in **a**. β-actin was used as a loading control. Representative result from two independent experiments. Gel source data are presented in Supplementary Fig. 1. **c**, Morphology (top), H&E staining (middle) and GFP immunofluorescence (bottom) in BAT from **a** (DAPI was used for counter staining). Scale bars, 100 μm. Representative result from two independent mice. **d**, Tissue temperature of BAT and muscle in **a** following treatment with noradrenaline (arrows). $n = 5$ (control), $n = 7$ (*Slc25a44*^{BAT}-KD). **e**, Rectal core body temperature of *Slc25a44*-KD ($n = 6$) and control ($n = 7$) mice following cold exposure at 8 °C. **f**, Val oxidation in indicated tissues normalized to tissue mass. $n = 4$ per group. **g**, Plasma BCAA levels in **e** following 8 h cold treatment at 8 °C. $n = 6$ per group. **h**, Noradrenaline-induced OCR normalized to total protein in control and *Slc25a44*-KO brown adipocytes. $n = 9$ per group (control + Val, *Slc25a44*-KO + Val + KIV), $n = 10$ per group (KO + Val, KO + Val + succinate). **i**, Val oxidation in inguinal WAT-derived white adipocytes expressing an empty vector or *Slc25a44* after noradrenaline treatment. $n = 5$ (vehicle), $n = 6$ (noradrenaline). **j**, A proposed model of BCAA catabolism in thermogenic adipose cells. Cold stimuli activate BCAA uptake and oxidation in the mitochondria of thermogenic adipocytes. Mitochondrial BCAA oxidation promotes BAT thermogenesis. This process requires SLC25A44, the mitochondrial BCAA transporter. SLC7A5, L-amino acid transporter 1. **a**, **d**–**i**, Biologically independent samples. Data are mean ± s.e.m.; two-sided *P* values by unpaired Student's *t*-test (**a**, **f**), one-way factorial (**h**) or two-way repeated measures ANOVA (**d**, **e**, **g**) followed by post hoc paired or unpaired *t*-test with Bonferroni's correction (**g**) or Tukey's test (**h**, **i**).

SLC25A44 is required for BCAA catabolism

To determine the role of SLC25A44 in vivo, we used a modified CRISPR system, using catalytically inactive Cas9 protein (dCas9) fused to Krüppel-associated box (KRAB) domain. Adeno-associated virus (AAV) expressing a guide RNA (gRNA) targeting *Slc25a44* or enhanced green fluorescent protein (eGFP; control) was injected into the interscapular BAT of dCas9-KRAB mice that were generated by the site-specific integrase-mediated approach[22] (Extended Data Fig. 8a–c). This system enabled BAT-selective knockdown of SLC25A44 (*Slc25a44*^{BAT}-KD) (Fig. 4a, b, Extended Data Fig. 8d, e). We found that brown adipocytes in *Slc25a44*^{BAT}-KD mice contained larger lipid droplets than those in control mice (Fig. 4c). Moreover, noradrenaline-induced BAT thermogenesis in *Slc25a44*^{BAT}-KD mice was significantly impaired relative to controls without affecting muscle thermogenesis (Fig. 4d). Next, we generated transgenic mice expressing gRNA-targeting *Slc25a44*, which were subsequently crossed with dCas9-KRAB mice to generate SLC25A44-deficient (*Slc25a44*-KD) mice (Extended Data Fig. 9a, b). Transcriptional analyses detected no compensatory change in other SLC25A members in *Slc25a44*-KD brown fat (Extended Data Fig. 9c, d). Similar to *Slc25a44*^{BAT}-KD mice, the BAT of *Slc25a44*-KD mice contained larger lipid droplets and higher levels of triglycerides compared with controls, whereas the morphology of WAT, liver, and muscle of *Slc25a44*-KD mice was normal (Extended Data Fig. 9e, f). Although we found no difference in the expression of *Ucp1* and genes associated with the fatty acid synthesis and oxidation pathway between the two groups, the core body temperature of *Slc25a44*-KD mice was significantly lower than in controls following cold exposure without affecting muscle shivering (Fig. 4e, Extended Data Fig. 9g–i). Tissue-temperature recording confirmed that noradrenaline-stimulated BAT thermogenesis was impaired in *Slc25a44*-KD mice (Extended Data Fig. 9j). Furthermore, Val oxidation in the BAT of *Slc25a44*-KD mice was lower than controls, indicating that SLC25A44 is the primary BCAA transporter in BAT (Fig. 4f). Of note, cold exposure failed to lower plasma BCAA concentration in *Slc25a44*-KD mice (Fig. 4g). These results indicate that SLC25A44 is required for cold-stimulated BAT thermogenesis and systemic BCAA clearance in vivo.

To determine the cell-autonomous function of SLC25A44 in brown adipocytes, we depleted *SLC25A44* in human brown preadipocytes using lentiviral shRNAs that target *SLC25A44* (Extended Data Fig. 10a, b). We found that *SLC25A44* depletion caused a significant reduction in noradrenaline-induced OCR in the presence of Val (Extended Data Fig. 10c, d). Supplementation with KIV or succinate, which bypasses mitochondrial BCAA transport, restored noradrenaline-induced OCR in *Slc25a44*-KO cells indicating that depletion of SLC25A44 did not cause a general mitochondrial defect (Fig. 4h, Extended Data Fig. 10e). In addition, SLC25A44-depleted brown adipocytes displayed active mitochondrial respiration (Extended Data Fig. 10f, g). Conversely,

overexpression of *Slc25a44* in mouse inguinal WAT-derived adipocytes or C2C12 myotubes significantly increased mitochondrial Val uptake and oxidation and cellular respiration (Fig. 4i, Extended Data Fig. 10h–m).

Discussion

The results of this study suggest the following model (Fig. 4j): in addition to glucose and fatty acids, cold stimuli potently increase mitochondrial BCAA uptake and oxidation in BAT, leading to enhanced BCAA clearance in the circulation. This process requires SLC25A44, a mitochondrial BCAA transporter in brown adipocytes. In turn, defective BCAA catabolism in BAT results in impaired BCAA clearance and thermogenesis, leading to the development of diet-induced obesity and glucose intolerance.

This model has important implications for the regulation of systemic BCAA metabolism in an obese or diabetic state, which results in impaired BAT activity and increased circulating BCAA in humans and rodents. It has been suggested that the accumulation of incompletely oxidized intermediates derived from BCAA oxidation, such as 3-hydroxyisobutyrate, causes insulin resistance[9,23,24]. Conversely, lowering circulating BCAA levels by inhibiting the kinase BDK or overexpression of the phosphatase PPM1K in the liver improves glucose tolerance independently for body-weight loss in rats[25]. Furthermore, reduced mitochondrial BCAA oxidation and subsequent intracellular accumulation of BCAA leads to constitutive activation of mTOR signalling, resulting in persistent IRS-1 phosphorylation by mTORC1 and inhibition of insulin signalling[6,23,26]. This study suggests a distinct yet non-mutually exclusive mechanism in which impaired BAT activity in conditions of obesity or diabetes reduces systemic BCAA clearance, whereas active BAT acts as a significant metabolic filter for circulating BCAA and protects against obesity and insulin resistance. Enhanced mitochondrial BCAA catabolism via SLC25A44 may serve as a promising strategy to improve systemic BCAA clearance and glucose homeostasis.

Online content

Any methods, additional references, Nature Research reporting summaries, source data, extended data, supplementary information, acknowledgements, peer review information; details of author contributions and competing interests; and statements of data and code availability are available at https://doi.org/10.1038/s41586-019-1503-x.

Received: 8 June 2018; Accepted: 22 July 2019;
Published online 21 August 2019.

1. Ouellet, V. et al. Brown adipose tissue oxidative metabolism contributes to energy expenditure during acute cold exposure in humans. *J. Clin. Invest.* **122**, 545–552 (2012).
2. Cypess, A. M. et al. Identification and importance of brown adipose tissue in adult humans. *N. Engl. J. Med.* **360**, 1509–1517 (2009).
3. Saito, M. et al. High incidence of metabolically active brown adipose tissue in healthy adult humans: effects of cold exposure and adiposity. *Diabetes* **58**, 1526–1531 (2009).
4. Bartelt, A. et al. Brown adipose tissue activity controls triglyceride clearance. *Nat. Med.* **17**, 200–205 (2011).
5. Chondronikola, M. et al. Brown adipose tissue activation is linked to distinct systemic effects on lipid metabolism in humans. *Cell Metab.* **23**, 1200–1206 (2016).
6. Newgard, C. B. et al. A branched-chain amino acid-related metabolic signature that differentiates obese and lean humans and contributes to insulin resistance. *Cell Metab.* **9**, 311–326 (2009).
7. Huffman, K. M. et al. Relationships between circulating metabolic intermediates and insulin action in overweight to obese, inactive men and women. *Diabetes Care* **32**, 1678–1683 (2009).
8. Wang, T. J. et al. Metabolite profiles and the risk of developing diabetes. *Nat. Med.* **17**, 448–453 (2011).
9. Lynch, C. J. & Adams, S. H. Branched-chain amino acids in metabolic signalling and insulin resistance. *Nat. Rev. Endocrinol.* **10**, 723–736 (2014).
10. Pietiläinen, K. H. et al. Global transcript profiles of fat in monozygotic twins discordant for BMI: pathways behind acquired obesity. *PLoS Med.* **5**, e51 (2008).
11. She, P. et al. Obesity-related elevations in plasma leucine are associated with alterations in enzymes involved in branched-chain amino acid metabolism. *Am. J. Physiol. Endocrinol. Metab.* **293**, E1552–E1563 (2007).
12. Lackey, D. E. et al. Regulation of adipose branched-chain amino acid catabolism enzyme expression and cross-adipose amino acid flux in human obesity. *Am. J. Physiol. Endocrinol. Metab.* **304**, E1175–E1187 (2013).
13. Herman, M. A., She, P., Peroni, O. D., Lynch, C. J. & Kahn, B. B. Adipose tissue branched chain amino acid (BCAA) metabolism modulates circulating BCAA levels. *J. Biol. Chem.* **285**, 11348–11356 (2010).
14. Neinast, M. D. et al. Quantitative analysis of the whole-body metabolic fate of branched-chain amino acids. *Cell Metab.* **29**, 417–429 (2019).
15. Shinoda, K. et al. Genetic and functional characterization of clonally derived adult human brown adipocytes. *Nat. Med.* **21**, 389–394 (2015).
16. Sustarsic, E. G. et al. Cardiolipin synthesis in brown and beige fat mitochondria is essential for systemic energy homeostasis. *Cell Metab.* **28**, 159–174 (2015).
17. Rosell, M. et al. Brown and white adipose tissues: intrinsic differences in gene expression and response to cold exposure in mice. *Am. J. Physiol. Endocrinol. Metab.* **306**, E945–E964 (2014).
18. Green, C. R. et al. Branched-chain amino acid catabolism fuels adipocyte differentiation and lipogenesis. *Nat. Chem. Biol.* **12**, 15–21 (2016).
19. Wallace, M. et al. Enzyme promiscuity drives branched-chain fatty acid synthesis in adipose tissues. *Nat. Chem. Biol.* **14**, 1021–1031 (2018).
20. Ohno, H., Shinoda, K., Ohyama, K., Sharp, L. Z. & Kajimura, S. EHMT1 controls brown adipose cell fate and thermogenesis through the PRDM16 complex. *Nature* **504**, 163–167 (2013).
21. Palmieri, F. The mitochondrial transporter family SLC25: identification, properties and physiopathology. *Mol. Aspects Med.* **34**, 465–484 (2013).
22. Tasic, B. et al. Site-specific integrase-mediated transgenesis in mice via pronuclear injection. *Proc. Natl Acad. Sci. USA* **108**, 7902–7907 (2011).
23. Newgard, C. B. Interplay between lipids and branched-chain amino acids in development of insulin resistance. *Cell Metab.* **15**, 606–614 (2012).
24. Jang, C. et al. A branched-chain amino acid metabolite drives vascular fatty acid transport and causes insulin resistance. *Nat. Med.* **22**, 421–426 (2016).
25. White, P. J. et al. The BCKDH kinase and phosphatase integrate BCAA and lipid metabolism via regulation of ATP-citrate lyase. *Cell Metab.* **27**, 1281–1293.e7 (2018).
26. Um, S. H., D'Alessio, D. & Thomas, G. Nutrient overload, insulin resistance, and ribosomal protein S6 kinase 1, S6K1. *Cell Metab.* **3**, 393–402 (2006).

Publisher's note: Springer Nature remains neutral with regard to jurisdictional claims in published maps and institutional affiliations.

© The Author(s), under exclusive licence to Springer Nature Limited 2019

METHODS

Human subjects. Thirty-three healthy young male volunteers were recruited in Sapporo, Japan to investigate the role of BAT in circulating BCAA clearance during cold exposure. All participants were carefully instructed regarding the study and provided written informed consent. The protocols were approved by the Institutional Research Ethics Review Board of Tenshi College (Sapporo, Japan) (UMIN000016361). Human BAT activity was assessed by ^{18}F-FDG-PET–CT scan (Aquiduo; Toshiba Medical Systems) after the standardized non-shivering cold exposure, as reported previously[27]. All the subjects have fasted for 12 h before ^{18}F-FDG-PET–CT scanning. Following cold exposure, the volunteers were given an intravenous injection of ^{18}F-FDG (1.66–5.18 MBq per kg (body weight)) and subsequently stayed in the same cold room for another 1 h. BAT activity was assessed by measuring the SUV of ^{18}F-FDG and Hounsfield Units from −300 to −10 in the supraclavicular region using Fusion software (Toshiba Medical Systems). On the basis of the median of BAT activity, subjects were divided into a high-BAT-activity group and a low-BAT-activity group. Arterialized blood samples were obtained from the same subject right before cold exposure and after 2 h cold exposure at 19 °C between 09:00 and 11:30. Sera were used for metabolite analysis. Amino acid levels were corrected for total amino acid levels by linear regression, since individual variation in the most of amino acids (85.3%) can be explained by total amino acids. To minimize possible effects of seasonal variation of BAT activities, the study was performed from January to March, during which the monthly average of ambient temperature in Sapporo was between −3.5 and 2.1 °C.

Animals. All the mouse experiments in this study were performed following the guidelines established by the UCSF Institutional Animal Care and Use Committee. Adult males and female mice aged 8–16 weeks had free access to food and water and were caged at 23 °C with 12-h light cycles and were used for the experiments. Mice were randomly assigned for the experimental groups at the time of purchase or weaning. For the generation of BAT-specific *Bckdha*-KO mice (*Bckdha*^{UCP1} mice), *Bckdha*-floxed mice were obtained from the European Mouse Mutant cell Repository (*Bckdha*$^{tm1a(EUCOMM)Hmgu}$) and crossed with *Ucp1-cre* mice[28]. For the generation of BAT-specific *Pparg*-KO mice, *Pparg*-floxed mice were obtained from the Jackson Laboratory (Stock #004584) and crossed with *Ucp1-cre* mice. Both knockout mice were on the C57BL/6 background.

For metabolic studies, male *Bckdha*^{UCP1}-KO and littermate control mice at eight weeks old were fed on a high-fat diet (HFD, 60% fat, D12492, Research Diets) at ambient temperature. Fat mass and lean mass were measured in mice on a high-fat diet for ten weeks by Body Composition Analyzer EchoMRI (Echo Medical Systems). For glucose tolerance test, the mice fed with high-fat diet for 10 weeks were fasted for 6 h (from 8:00 to 14:00) and injected intraperitoneally with glucose (1.5 g per kg (body weight)). For insulin tolerance test (ITT) experiments, the mice fed with high-fat diet for 11 weeks were fasted for 3 h (from 10:00 to 13:00) and injected intraperitoneally with insulin (0.875 U per kg (body weight)). Blood samples were collected at the indicated time points, and glucose levels were measured using blood glucose test strips (Abbott). BCAA tolerance test was performed in male *Bckdha*^{UCP1}-KO and control mice on a high-fat diet for ten weeks. For BCAA clearance test, mice were exposed to cold temperature under the fasting condition, and blood samples were obtained at the indicated time points. For BCAA tolerance test, mice were received a single bolus of BCAA oral gavage (500 mg per kg (body weight); weight ratio: Val:Leu:Ile, 1: 1.5: 0.8)[29] and were exposed to cold at 12 °C under the fasting condition. Blood was collected at the indicated time points and total plasma BCAA levels were measured by using a commercially available kit (ab83374, Abcam). Independently, plasma BCAA levels after 3 h oral BCAA gavage were quantified by flow-injection electrospray-ionization tandem mass spectrometry and quantified by isotope-dilution technique using a method described previously[30]. In brief, plasma samples were spiked with a cocktail of heavy-isotope internal standards (Cambridge Isotope Laboratories; CDN Isotopes), deproteinated with methanol, and esterified with butanol. Mass spectra for amino acid esters were obtained using neutral loss scanning methods. Ion ratios of analyte to the respective internal standard computed from centroided spectra were converted to concentrations using calibrators constructed from authentic amino acids (Sigma; Larodan) and dialysed fetal bovine serum (Sigma).

dCas9-KRAB mice were generated according to the method reported using a site-specific integrase-mediated approach as described[22]. In brief, transgenic mice dCas9-KRAB on the FVB background contain a CAG promoter within the *Hipp11* (H11) locus expressing the nuclease-deficient Cas9 fused to the zinc-finger protein 10 (ZNF10) Krüppel-associated box (KRAB) repressor domain[31], together with mCherry and the puromycin resistance cassette. dCas9-KRAB mice were backcrossed with wild-type C57BL/6J mice and subsequently crossed with gRNA-*Slc25a44* transgenic mice to generate *Slc25a44*-KD mice.

BAT-specific *Slc25a44*-KD (*Slc25a44*^{BAT}-KD) mice were generated by injecting adeno-associated virus (AAV) expressing gRNA-*Slc25a44* (AAV8-CAG-eGFP-U6-gRNA-long tracr; custom order, Vector Biolabs) or control GFP (AAV8-CAG-eGFP) into interscapular BAT following the published protocol[32]. In short, AAV was injected into the interscapular BAT of dCas9-KRAB adult mice at a viral titer of 6.0×10^{11} genomic copies (GC) per mouse. Fifty microlitres of AAV at a dose of 1.2×10^{10} GC μl^{-1} was injected in each BAT depot (5 μl per injection, 10 locations per depot). Efficacy of viral infection and knockdown was evaluated by immunohistochemistry for GFP and quantification of SLC25A44 expression level.

Chemicals and antibodies. All chemicals were obtained from Sigma-Aldrich unless otherwise specified. The following antibodies were used in this study: UCP1 antibody (ab-10983, Abcam), BCAT1 antibody (TA504360, OriGene), BCAT2 antibody (9432, Cell Signaling Tech), BCKDHA antibody (sc-271538, Santa Cruz), TOM20 antibody (11802-1-AP, Proteintech), COX-IV antibody (4850, Cell Signaling), OXPHOS cocktail (Abcam, ab110413), PDH-E1α antibody (sc-377092, Santa Cruz), PDH-E1α (pSer232) antibody (AP1063, Millipore), PDH-E1α (pSer293) antibody (ab177461, Abcam), PDH-E1α (pSer300) antibody (AP1064, Millipore), GAPDH antibody (sc-32233, Santa Cruz) and β-actin antibody (A3854, Sigma-Aldrich). Polyclonal antibody for SLC25A44 was generated by using the peptides (MEDKRNIQIIEWEHLDKKKC, MMQRKGEKMGRFQVC and CKKLSLRPELVDSRH) as epitopes for immunization in rabbit (GeneScript).

Cell culture. Brown adipocyte and beige adipocyte lines from C57BL/6 mice were established in our previous study[33]. Similarly, immortalized human brown adipocyte and white adipocyte lines were established previously[15]. Mouse adipocyte differentiation was induced by treating confluent preadipocytes with DMEM containing 10% FBS, 0.5 mM isobutylmethylxanthine, 125 nM indomethacin, 2 μg ml^{-1} dexamethasone, 850 nM insulin, 1 nM T3 and 0.5 μM rosiglitazone. Two days after induction, cells were switched to maintenance medium containing 10% FBS, 850 nM insulin, 1 nM T3 and 0.5 μM rosiglitazone. Mouse cells were fully differentiated 6–7 days after inducing differentiation. Immortalized human brown preadipocytes were cultured with animal component-free medium (Stem Cell Technologies; #05449). Brown adipocyte differentiation was induced by treating confluent preadipocytes with animal component free adipogenic differentiation medium (Stem Cell Technologies; #05412) supplemented with T3 (1 nM) and rosiglitazone (0.5 μM). Human cells were fully differentiated four weeks after induction. Mouse embryonic fibroblasts (MEF) were isolated from dCas9-KRAB mice and immortalized by infecting retrovirus expressing SV-Large T antigen. A mouse neuroblastoma line, Neuro2a (89121404, Sigma-Aldrich), was cultured in minimum essential medium Eagle (Sigma-Aldrich, M4655) containing 10% FBS, 1% non-essential amino acid solution (Sigma-Aldrich, M7145) and 1% penicillin–streptomycin solution on collagen-coated plates. C2C12 cells were differentiated into myotubes by culturing confluent cells with DMEM supplemented with 2% FBS and 850 nM insulin. HEK293S cells were infected with retrovirus expressing the C-terminal Flag-tagged *Slc25a44* or an empty vector and cultured in suspension with a FreeStyle 293 Expression Medium (Thermo Fisher; 12338018) supplemented with 2% FBS. HEK293 and C2C12 cells were purchased from ATCC. No commonly misidentified cell line was used in this study. All the cell lines were routinely tested negative for mycoplasma contamination.

Stable-isotope-labelled Leu metabolome analysis. To determine the metabolic fate and catabolic flux of Leu in brown adipocytes, we used [^{13}C$_6$, ^{15}N$_1$]Leu tracing followed by CE-TOFMS (Agilent Technologies). Differentiated human brown adipocytes were incubated in the BCAA-free medium supplemented with 2 mM [^{13}C$_6$, ^{15}N$_1$]Leu (608068, Sigma-Aldrich) and collected 1 h after the treatment with noradrenaline, washed twice with 10 ml of 5% mannitol aqueous solution, and subsequently incubated with 1 ml of methanol containing 25 μM internal standards (methionine sulfone, 2-(*N*-morpholino)-ethanesulfonic acid (MES) and D-camphor-10-sulfonic acid) for 10 min. Four hundred microlitres of the extracts were mixed with 200 μl Milli-Q water and 400 μl chloroform and centrifuged at 10,000*g* for 3 min at 4 °C. Subsequently, 400 μl of the aqueous solution was centrifugally filtered through a 5-kDa cut-off filter (Human Metabolome Technologies) to remove proteins. The filtrate was centrifugally concentrated and dissolved in 50 μl of Milli-Q water that contained reference compounds (200 μM each of 3-aminopyrrolidine and trimesate) immediately before metabolome analysis.

The concentrations of all the charged metabolites in samples were measured by CE-TOFMS, following the methods as previously reported[34]. In brief, a fused silica capillary (50 μm internal diameter × 100 cm) was used with 1 M formic acid as the electrolyte. Methanol:water (50% v/v) containing 0.1 μM hexakis (2,2-difluoroethoxy) phosphazene was delivered as the sheath liquid at 10 μl min^{-1}. Electrospray ionization (ESI)-TOFMS was performed in positive-ion mode, and the capillary voltage was set to 4 kV. Automatic recalibration of each acquired spectrum was achieved using the masses of the reference standards [(^{13}C isotopic ion of a protonated methanol dimer (2 MeOH + H)]$^+$, *m*/*z* 66.0632) and ([hexakis (2,2-difluoroethoxy) phosphazene + H]$^+$, *m*/*z* 622.0290). Quantification was performed by comparing peak areas to calibration curves generated using internal standardization techniques with methionine sulfone. The other conditions were identical to those described previously[34]. To analyse anionic metabolites, a commercially available COSMO(+) (chemically coated with cationic polymer) capillary (50 μm internal diameter × 105 cm) (Nacalai Tesque) was used with a

50 mM ammonium acetate solution (pH 8.5) as the electrolyte. Methanol–5 mM ammonium acetate (50% v/v) containing 0.1 μM hexakis (2,2-difluoroethoxy) phosphazene was delivered as the sheath liquid at 10 μl min^{-1}. ESI-TOFMS was performed in negative ion mode, and the capillary voltage was set to 3.5 kV. For anion analysis, trimesate and CAS were used as the reference and the internal standards, respectively. The other conditions were identical to those described previously[35]. MPE of isotopes, an index of isotopic enrichment of metabolites, was calculated as the percent of all atoms within the metabolite pool that are labelled according to the established formula[18,19]

DNA constructs for overexpression and knockdown studies. The lentiviral expression plasmid that encodes mouse *Slc25a44* open reading frame was obtained from GeneCopoeia (EX-Mm15289-Lv207-GS). The *Slc25a44* sequence was amplified from the lentiviral plasmid by PCR and cloned in-frame with a Flag sequence into the retroviral expression vector (Addgene, #75085). Lentiviral shRNA expression constructs targeting mouse *Slc25a44* and *Slc25a39* (sh*Slc25a44*, CS-MSH073484-LVRU6GH-01; sh*Slc25a39*, MSH034465-LVRU6GH; scrambled control, CSHCTR001-LVRU6GH), lentiviral shRNA expression constructs targeting human *SLC25A44* (sh*SLC25A44*, HSH057134-LVRH1H; scrambled control, CSHCTR001-LVRH1H), as well as lentiviral shRNA expression construct targeting mouse *Ucp1* were obtained from GeneCopoeia (sh*Ucp1*, MSH028473-LVRH1MH). For virus production, HEK293T packaging cells were transfected with 10 μg of lentiviral or retroviral plasmids and the packaging constructs (VSVg, pMDL, and Rev) using a calcium phosphate method. After 48 h, the viral supernatant was collected and filtered. Immortalized preadipocytes, Neuro2a or HEK293S cells were incubated overnight with the viral supernatant and supplemented with 10 μg ml^{-1} polybrene. Hygromycin at a dose of 50 or 200 μg ml^{-1} was used for selection of lentivirus-infected human cells and murine cells, respectively. Blasticidin at a dose of 10 μg ml^{-1} was used for selection of retrovirus-infected cells.

Generation of *Bckdha*-KO and *Slc25a44*-KO brown adipocytes. For generation of *Bckdha*-KO brown adipocytes, preadipocytes isolated from BAT of *Bckdha*$^{flox/flox}$ mice were immortalized by using the SV40 Large T antigen as described previously[15] and subsequently infected with retrovirus containing Cre (#34565, Addgene), followed by hygromycin selection at a dose of 200 μg ml^{-1}. For generation of *Slc25a44*-KO brown adipocytes, immortalized brown adipocyte cell line was infected with lentivirus packaged by lentiCRISPRv2 (#98291, Addgene) expressing Cas9 and gRNA for *Slc25a44* (5′-GGTGCTCCCACTCGATGATC-3′). After selection with 200 μg ml^{-1} hygromycin followed by isolating a monoclonal cell, we confirmed homozygous mutations in the *Slc25a44* genes by DNA sequencing.

RNA preparation, quantitative RT–PCR and RNA-sequencing. Total RNA was extracted from tissue or cells using RNeasy mini-kit (Qiagen) and cDNA was synthesized using iScript cDNA Synthesis kit (BioRad) according to the provided protocols. qRT–PCR was performed using an ABI ViiA7 PCR cycler. The primer sequences are listed in Supplementary Table 4. For RNA-sequencing, the libraries were constructed from total RNA and sequenced using a HiSeq 3000 instrument (Illumina) at the UCLA Technology Center for Genomics and Bioinformatics core by technical staff who were blinded to the experimental group. Sequenced tags were pseudo-aligned to mouse reference transcriptome. Transcript-levels estimated using Kallisto 0.44.0 were imported into R and expression levels per gene were estimated using the Bioconductor package tximport 1.10.0.

BCAA oxidation assay. Differentiated adipocytes in a six-well plate were washed with PBS and incubated in 1 ml Krebs–Ringer modified buffer (KRB)–HEPES buffer, containing 2% BSA, 15 mM glucose, 200 nM adenosine, and either 0.16 μCi ml^{-1} [1-^{14}C]Val together with 1 mM non-radioisotope (RI) Val or 0.16 μCi ml^{-1} [1-^{14}C]Leu together with non-RI 1 mM Leu, at 37 °C for 2 h. Subsequently, 350 μl 30% hydrogen peroxide was added in each well, and [^{14}C]CO_2 was trapped in the smears supplemented with 300 μl of 1 M benzethonium hydroxide solution at room temperature for 20 min. Similarly, isolated tissue (20–30 mg) was placed in a plypropylene round-bottom tube and incubated in the 1 ml KRB–HEPES buffer containing 0.16 μCi ml^{-1} [1-^{14}C]Val at 37 °C for 1 h. After adding 350 μl 30% hydrogen peroxide in the tube, [^{14}C]CO_2 was trapped in the centre well supplemented with 300 μl of 1 M benzethonium hydroxide solution for 20 min at room temperature. BCAA oxidation was quantified by counting radioactivity of trapped [^{14}C]CO_2 using a scintillation counter.

Mitochondrial amino acid uptake assay. Differentiated adipocytes in 10 cm culture plates were washed in cold PBS and incubated with KPBS at 4 °C for 10 min. Confluent Neuro2a cells were incubated with KPBS without washing in PBS to minimize cell loss. After removing KPBS, mitochondria were isolated by using a mitochondria isolation kit (Thermo Fisher; 89874) according to the provided protocol. Isolated mitochondria were incubated with KRB–HEPES buffer, containing 2% BSA, 15 mM glucose, 200 nM adenosine, and either 0.32 μCi ml^{-1} [U-^{14}C] Val, [U-^{14}C]Leu, [U-^{14}C]Ala, [U-^{14}C]Phe, [U-^{14}C]Thr, [U-^{14}C]Glu, [U-^{14}C]Asp, [U-^{14}C]Lys, [U-^{14}C]Arg (Moraveck), or [1-^{14}C]α-ketoisovalerate (American Radiolabelled Chemicals) at 37 °C for 1 h. After cooling down on ice, mitochondria were washed in chilled PBS three times and homogenized in 100 μl RIPA buffer. Mitochondrial amino acid uptake was quantified by counting radioactivity using a scintillation counter and normalized to protein content.

Liposome preparation. Egg phosphatidylcholine (1.280 ml, 25 mg ml^{-1} in $CHCl_3$, Avanti Polar Lipids, 840051), *E.coli* polar lipid (1.344 ml, 25 mg ml^{-1} in $CHCl_3$, Avanti Polar Lipids, 100600), and cardiolipin (0.640 ml, 10 mg m^{-1} in $CHCl_3$, Sigma-Aldrich, C0563) were mixed in round-bottomed flask. The solvent was removed by rotary evaporation under vacuum at room temperature to form a lipid film, and further dried under strong vacuum for at least 2 h to remove trace $CHCl_3$. Four millilitres of 10 mM PIPES buffer pH7.4, which contains 25 mM non-radioisotope Leu and Glu as internal substrates, was gently added to the dried lipid film. The flask was kept overnight at 4 °C to allow the formation of large unilamellar vesicles (LUVs), followed by incubating at 70 °C for 30 min. The LUVs were extruded seven times through an extruder (Avanti Polar Lipids, 610000), which was assembled with two drain disks separated with a 1.0-μm-pore polycarbonate membrane (GE Whatman, 889-78159). The extruded liposome was concentrated to 40 mg ml^{-1} lipid concentration in 10-kDa centrifugal filters (Millipore, UFC505024).

Mitochondrial liposome assay. Mitochondria were isolated from differentiated *Slc25a44*-KO brown adipocytes stably expressing either *Slc25a44* or an empty vector (90 plates per group). The mitochondrial membrane was obtained by mechanical disruption and sonication. Sonicated mitochondrial membranes (2 mg ml^{-1}) were fused with liposome (4 mg ml^{-1}) by incubating with 40 mM β-D-octyl glucoside (β-OG, Sigma-Aldrich, O8001) at 4 °C for 1 h in PIPES buffer containing non-radioactive Leu and Glu. After removal of β-OG by Bio-Beads SM-2 (Bio-Rad), mitochondrial liposomes were isolated on Sepharose 4B columns (Sigma-Aldrich, 4B-200) to remove the external substrates. Mitochondrial liposomes were trapped on 10-kDa centrifugal filters (Millipore, UFC505024), eluted in 1200 μl PIPES buffer without non-radioactive Leu or Glu, and then used for uptake assays. Transport of [$^{14}C_6$]Leu or [$^{14}C_5$]Glu was initiated by incubating mitochondrial liposomes with either 20 μM [$^{14}C_6$]Leu or 20 μM [$^{14}C_5$]Glu at 37 °C and stopped by filtering the reaction mixture with a vacuum manifold (0.45-μm pore size) at the indicated time points. Following six washes with 600 μl ice-cold PIPES buffer, uptake was quantified with a scintillation counter.

Proteoliposome assay. HEK293S cells stably expressing C-terminal Flag-tagged *Slc25a44* were cultured in 9 l suspension medium, collected and disrupted with a Dounce homogenizer in solubilization buffer (20 mM Tris-HCl, 100 mM NaCl, 10% glycerol, 1% DDM with 0.1% cholesteryl hemisuccinate (CHS, Anatrace, D310-CH210), EDTA-free protease inhibitor (Roche)), followed by solubilization at 4 °C for 1 h. After ultracentrifugation at 200,000*g* for 20 min, the supernatant was incubated with Flag M2 affinity gel (Sigma-Aldrich, A2220) at 4 °C for 2 h. The immunoprecipitates were washed five times with washing buffer (20 mM Tris-HCl, 500 mM NaCl, 10% glycerol, 0.1% DDM with 0.01% CHS), followed by competitive elution using Flag peptide (Sigma-Aldrich, F4799) in SEC buffer (20mM Tris-HCl, 100 mM NaCl, 10% glycerol, 0.1% DDM with 0.01% CHS). Purified SLC25A44–Flag (56 μg) was fused with liposome (8 mg) by incubating at 4 °C for 1 h in 2 ml PIPES buffer containing 25 mM non-radioactive Leu and Glu in the presence of 40 mM β-OG. Following removal of β-OG by Bio-Beads SM-2, proteoliposome was isolated on Sepharose 4B columns to remove the external substrates. Subsequently, the proteoliposomes were trapped on 10-kDa centrifugal filters, eluted in 1200 μl PIPES buffer without non-radioactive Leu or Glu, and then used for uptake assays. Transport of [$^{14}C_6$]Leu was initiated by incubating proteoliposomes with 20 μM [$^{14}C_6$]Leu at 37 °C and stopped by filtering the reaction mixture with vacuum manifold at the indicated time points. Following six washes with 600 μl ice-cold PIPES buffer, uptake was quantified by a scintillation counter.

Temperature recording. For core-body temperature recording experiments, rectal temperature of *Bckdha*^{UCP1}-KO and *Slc25a44*-KD mice was monitored using a TH-5 thermometer (Physitemp) up to 14 h after cold exposure. For tissue temperature recording, mice under anaesthesia were implanted with type T thermocouple probes in the interscapular BAT, inguinal WAT, liver, and skeletal muscle, according to the method that was described previously[33]. Tissue temperature was recorded by TC-2000 Meter (Sable Systems International). When tissue temperature was stable, mice were intraperitoneally administered noradrenaline at a dose of 1 mg per kg (body weight) to induce non-shivering thermogenesis.

Electromyography. Skeletal muscle shivering was assessed by using electromyography (EMG) recording, as reported in our previous study[33]. In brief, mice were placed in a restrainer to limit free movement, and 29-gauge needle electrodes were placed the back muscles of mice. The EMG signal was processed (low-pass filter, 3 kHz; high-pass filter,10 Hz; notch filter, 60 Hz) and amplified 1,000 × with Bio Amp (ADInstruments). EMG data were collected from the implanted electrodes at a sampling rate of 2 kHz using LabChart 8 Pro Software (ADInstruments). The raw signal was converted to root mean square (RMS) activity. RMS activity was analysed for shivering bursts in 10-s windows. For monitoring muscle shivering in humans, EMG at the pectoral muscle was recorded by using a surface EMG (Polymate II; TEAC). EMG was recorded for 10 min at 27 °C before cold exposure, and for another 10 min at 19 °C during the 2 h cold exposure.

^{18}F-Fluciclovine-PET–CT scan. ^{18}F-Fluciclovine (100 μCi) was administered to male wild-type mice (C57Bl6/J) at 14–15 weeks of age via a tail-vein injection under 2% isoflurane anaesthesia after 6 h fasting. Mice were acclimatized to either 30 °C or cold temperature at 15 °C for 2 weeks. ^{18}F-Fluciclovine-uptake (SUV) was measured every minute immediately after tail vein injection using micro-PET–CT imaging system at the UCSF PET–CT Imaging Core Facility. Changes in SUV were quantified starting from the first 60 s after ^{18}F-Fluciclovine injection by using software AMIDE 1.0.4 (Amide).

Oxygen consumption assays. OCR in cultured adipocytes was measured using the Seahorse XFe Extracellular Flux Analyzer (Agilent) in a 24-well plate. For measurement of noradrenaline-induced respiration in the presence and absence of BCAA, differentiated adipocytes were maintained in KRB–HEPES buffer containing 15 mM glucose, 200 nM adenosine, and 2% BSA. During OCR measurement, cells were treated with 2 mM BCAA (Val, Leu, or Ile), 2 mM KIV, 10 mM succinate, or vehicle, and subsequently treated with noradrenaline (1 μM) at the indicated time point. For the mitochondrial stress test, differentiated brown adipocytes in a 24-well plate were pretreated with 300 μM clofibrate, a BCAT2 activator, and subjected to respiratory assay. During OCR measurement, cells were treated with oligomycin (5 μM), carbonyl cyanide 4-(trifluoromethoxy) phenylhydrazone (FCCP, 5 μM) and antimycin (5 μM).

Mitochondrial electron transport activity. Mitochondrial electron transport (ETC) activity was assessed as reported previously[36]. In brief, mitochondria were isolated from BAT of mice using a Comitial Kit (Ab110168, Abcam) and were resuspended in 300 μl of isolation buffer provided by the kit. After protein quantification by the BCA method, the mitochondrial suspension was diluted with isolation buffer at concentration 0.1 mg ml^{-1}, seeded into a 24-well plate (5 μg per 50 μl per well), and adhered to the bottom of the plate by centrifugation 2,000*g* at 4 °C for 20 min using microplate rotor adaptor. Immediately before the measurement, 450 μl mitochondrial assay buffer and substrates supplemented with 10 mM pyruvate, 5 mM malate, 50 mM KCl, 4 mM KH_2PO_4, 5 mM HEPES, 1 mM EGTA and 4% fatty-acid-free BSA was added to each well. During OCR measurement by the Seahorse XFe Extracellular Flux Analyzer, mitochondria were treated with 2 μM rotenone, 10 mM succinate, 5 μM antimycin A and 100 μM *N*,*N*,*N*′,*N*′-tetramethyl-*p*-phenylenediamine (TMPD) with 10 mM ascorbate at the indicated time points.

PDH activity and BCKDH activity assays. Tissue lysate was prepared by homogenizing BAT in ice-cold PBS buffer containing cOmplete Protease Inhibitor Cocktail (Roche) and 5 mM NaF. Two hundred micrograms of BAT lysates were applied to measure PDH enzymatic activities by a commercially available kit (Abcam, ab109902). The BCKDH activity measurement was performed as previously described[37].

Glucose oxidation assay. Differentiated adipocytes in a six-well plate were incubated in DMEM containing 2% FBS for 2 h. After washing in PBS, cells were incubated in 1 ml of KRB–HEPES buffer containing 2% BSA, 15 mM glucose, 200 nM adenosine, and 0.5 μCi ml^{-1} [1-^{14}C]glucose, supplemented with or without 1 mM Val, at 37 °C for 2 h. Subsequently, 350 μl 30% hydrogen peroxide was added in each well, and [^{14}C]CO_2 was trapped in the smears supplemented with 300 μl 1 M benzethonium hydroxide solution at room temperature for 20 min. For the assay in tissues, mice were fasted for 6 h and euthanized. Isolated tissue (20–30 mg) was placed in a plypropylene round-bottom tube and incubated in the 1 ml KRB/HEPES buffer containing 1.0 μCi ml^{-1} [1-^{14}C]glucose at 37 °C for 1 h. After adding 350 μl 30% hydrogen peroxide in the tube, [^{14}C]CO_2 was trapped in the centre well supplemented with 300 μl of 1 M benzethonium hydroxide solution for 20 min at room temperature. Glucose oxidation was quantified by counting radioactivity of trapped [^{14}C]CO_2 using a scintillation counter.

Fatty acid oxidation assay. Differentiated adipocytes were plated in a six-well plate and incubated in medium containing 2% FBS for 4 h. After washing in PBS, the cells were incubated in 1 ml of KRB–HEPES buffer, containing 15 mM glucose, 0.1 mM oleic acid, and 0.5 μCi ml^{-1} [1-^{14}C]oleic acid bound to 2% BSA and 100 μM carnitine, supplemented with or without 1 mM Val, for 2 h at 37 °C. Then, 350 μl 30% hydrogen peroxide was added in each well to trap [^{14}C]CO_2 in the smears supplemented with 300 μl of 1 M benzethonium hydroxide solution. For the assay in tissues, mice were fasted for 4 h and euthanized. Isolated tissue (20–30 mg) was placed in a polypropylene round-bottom tube and incubated in the 1 ml KRB–HEPES buffer containing 1.0 μCi ml^{-1} [1-^{14}C]oleic acid at 37 °C for 1 h. After adding 350 μl 30% hydrogen peroxide in the tube, [^{14}C]CO_2 was trapped in the centre well supplemented with 300 μl of 1 M benzethonium hydroxide solution for 20 min at room temperature. Oleic acid oxidation was quantified by counting radioactivity of trapped [^{14}C]CO_2 using a scintillation counter.

Immunoblotting. Protein lysates from isolated tissues or cultured cells were extracted using Qiagen TissueLyzer LT and RIPA lysis and extraction buffer (Thermo Fisher) and cOmplete protease inhibitors (Roche). Tissue lysates were applied to immunoblot analysis using the UCP1 antibody (1:2,000), BCAT1 antibody (1:1,000), BCAT2 antibody (1:1,000), BCKDHA antibody (1:2,000), TOM20 antibody (1:2,000), COX-IV antibody (1:2,000), OXPHOS cocktail (1:2,000), PDH-E1α antibody (1:1,000), PDH-E1α (pSer232) antibody (1:1,000), PDH-E1α (pSer293) antibody (1:1,000), PDH-E1α (pSer300) antibody (1:1,000), and SLC25A44 antibody (1:1,000). β-actin (1:10,000) and GAPDH (1:2,000) were used as a loading control for each sample.

Tissue histology and immunostaining. For H&E staining, tissues of mice were fixed in 4% paraformaldehyde overnight at 4 °C, followed by dehydration in 70% ethanol. After the dehydration procedure, tissues were embedded in paraffin, sectioned at a thickness of 5 μm, and stained with H&E following the standard protocol. For immunostaining, paraffin-embedded tissues were deparaffinized twice in xylene and subsequently rehydrated. After incubating the slides for 20 min in boiling water, the tissues were blocked in PBS containing 2% BSA for 60 min. After washing in PBS, the slides were incubated with the primary antibody (chicken anti-mouse GFP, 1:200) overnight at 4 °C, followed by incubation with the fluorescence-conjugated second antibody (goat anti-chicken IgG Alexa Fluor 488 green, 1:500) for 1 h at room temperature. After washing, the sections were stained with DAPI and mounted with mounting medium (Cytoseal 60, Thermo-Scientific). Images of tissue samples were captured using the Inverted Microscope Leica DMi8.

Statistical analyses. All data were expressed as mean ± s.e.m. and analysed with statistical software (SPSS 25.0; IBM). The sample size was determined by the power analysis with $\alpha = 0.05$ and power of 0.8, and based on our experience with experimental models, anticipated biological variables and previous studies. The metabolite analyses in human sera and mouse plasma, the [$^{13}C_6$, $^{15}N^1$]Leu tracing in human brown adipocytes, the PET–CT examination using ^{18}F-FDG (in humans) or ^{18}F-fluciclovine (in mice), and GTT and ITT in mice fed high-fat diet were performed by researchers who were blinded to the experimental groups. RNA sequencing and library constructions were performed by technical staff at the UCLA genome core who were blinded to the experimental groups. RNA sequencing alignment were performed by researchers who were blinded to the experimental groups. Blinding was not relevant to the other experiments in mice or cells because mice or cells had to be genotyped by PCR. Comparisons between the two groups were analysed using the paired *t*-test or the Student's *t*-test, as appropriate. One-way or two-way ANOVA followed by Tukey's post hoc test or post hoc paired/unpaired *t*-tests with Bonferroni's correction was used for multiple group comparisons. One-way or two-way repeated measures ANOVA was used for the comparisons of repeated measurements. Pearson's and Spearman's correlation coefficients were used to determine normally distributed variables and non-normally distributed variables, respectively. One-tailed paired *t*-test was used to analyse qRT–PCR validation of human BAT biopsy RNA-seq data. For all other experiments, two-tailed *P* value was calculated; $P<0.05$ was considered statistically significant.

Reporting summary. Further information on research design is available in the Nature Research Reporting Summary linked to this paper.

Data availability

The RNA-seq data generated in this study are available at Array Express under the accession code E-MTAB-7987. ^{13}C-Leu tracing data are available in Supplementary Table 3. Uncropped immunoblot images are available in Supplementary Fig. 1. The other datasets that support the findings of this study are available in Supplementary Information and Source Data.

27. Yoneshiro, T. et al. Recruited brown adipose tissue as an antiobesity agent in humans. *J. Clin. Invest.* **123**, 3404–3408 (2013).
28. Kong, X. et al. IRF4 is a key thermogenic transcriptional partner of PGC-1α. *Cell* **158**, 69–83 (2014).
29. Li, T. et al. Defective branched-chain amino acid catabolism disrupts glucose metabolism and sensitizes the heart to ischemia–reperfusion injury. *Cell Metab.* **25**, 374–385 (2017).
30. Ferrara, C. T. et al. Genetic networks of liver metabolism revealed by integration of metabolic and transcriptional profiling. *PLoS Genet.* **4**, e1000034 (2008).
31. Gilbert, L. A. et al. CRISPR-mediated modular RNA-guided regulation of transcription in eukaryotes. *Cell* **154**, 442–451 (2013).
32. Balkow, A. et al. Direct lentivirus injection for fast and efficient gene transfer into brown and beige adipose tissue. *J. Biol. Methods* **3**, e48 (2016).
33. Ikeda, K. et al. UCP1-independent signaling involving SERCA2b-mediated calcium cycling regulates beige fat thermogenesis and systemic glucose homeostasis. *Nat. Med.* **23**, 1454–1465 (2017).
34. Soga, T. et al. Differential metabolomics reveals ophthalmic acid as an oxidative stress biomarker indicating hepatic glutathione consumption. *J. Biol. Chem.* **281**, 16768–16776 (2006).
35. Soga, T. et al. Metabolomic profiling of anionic metabolites by capillary electrophoresis mass spectrometry. *Anal. Chem.* **81**, 6165–6174 (2009).
36. Das, K. C. Hyperoxia decreases glycolytic capacity, glycolytic reserve and oxidative phosphorylation in MLE-12 cells and inhibits complex I and II function, but not complex IV in isolated mouse lung mitochondria. *PLoS One* **8**, e73358 (2013).
37. White, P. J. et al. Branched-chain amino acid restriction in Zucker-fatty rats improves muscle insulin sensitivity by enhancing efficiency of fatty acid oxidation and acyl-glycine export. *Mol. Metab.* **5**, 538–551 (2016).

Acknowledgements We thank C. B. Newgard for the initial metabolomics analysis, E. Kunji for liposome study, Y. Seo and T. Huynh for the PET–CT scan, Y. Cheng and E. Green for HEK293S cells, E. T. Chouchani and E. Mills for cell respiration studies, and X. Lu and K. Shinoda for technical help. This work was supported by the NIH (DK97441 and DK112268) and the Edward Mallinckrodt Jr. Foundation to S.K., the American Diabetes Association Pathways Award (1-16-INI-17) to P.J.W., the AMED–CREST from the Japan Agency for Medical Research and Development to T.S., and the NIH (U19CA179513 and P30 DK063720) to M.T.M. T.Y. and M.K. are supported by the JSPS Fellowships.

Author contributions T.Y. designed and carried out overall experiments and analysed data. Q.W. designed and performed cellular experiments and liposome assays and interpreted data. K.T. and C.H.S. performed mouse experiments. M.M. and M.C. carried out human studies and analysed the data with M.S. and L.S. H. Maki, K. Igarashi, A.U. and M.O. performed BCAA-tracing studies and analysed the data with T.S. Z.D., M.K., H.L. and H. Majd performed liposome assays and analysed the data with F.C.S. P.J.W., R.W.M., O.R.I. and Y.D. measured amino acids in mice and BCKDH activity. Y.O., K. Ikeda, K.K., Y.C., M.Y. and Z.B. assisted with mouse experiments and cultured cell studies. R.N.P. conducted RNA-sequencing analysis. V.J.G. and M.T.M. developed dCas9–KRAB mice. H.T., T.G. and T.K. assisted with quantification of metabolites in human sera. S.K. conceived the project and directed the research. S.K. and T.Y wrote the paper with input from all the authors.

Competing interests The authors declare no competing interests.

Additional information

Supplementary information is available for this paper at https://doi.org/10.1038/s41586-019-1503-x.

Correspondence and requests for materials should be addressed to S.K.

Peer review information *Nature* thanks Ferdinando Palmieri, Yibin Wang and the other, anonymous, reviewer(s) for their contribution to the peer review of this work.

Reprints and permissions information is available at http://www.nature.com/reprints.

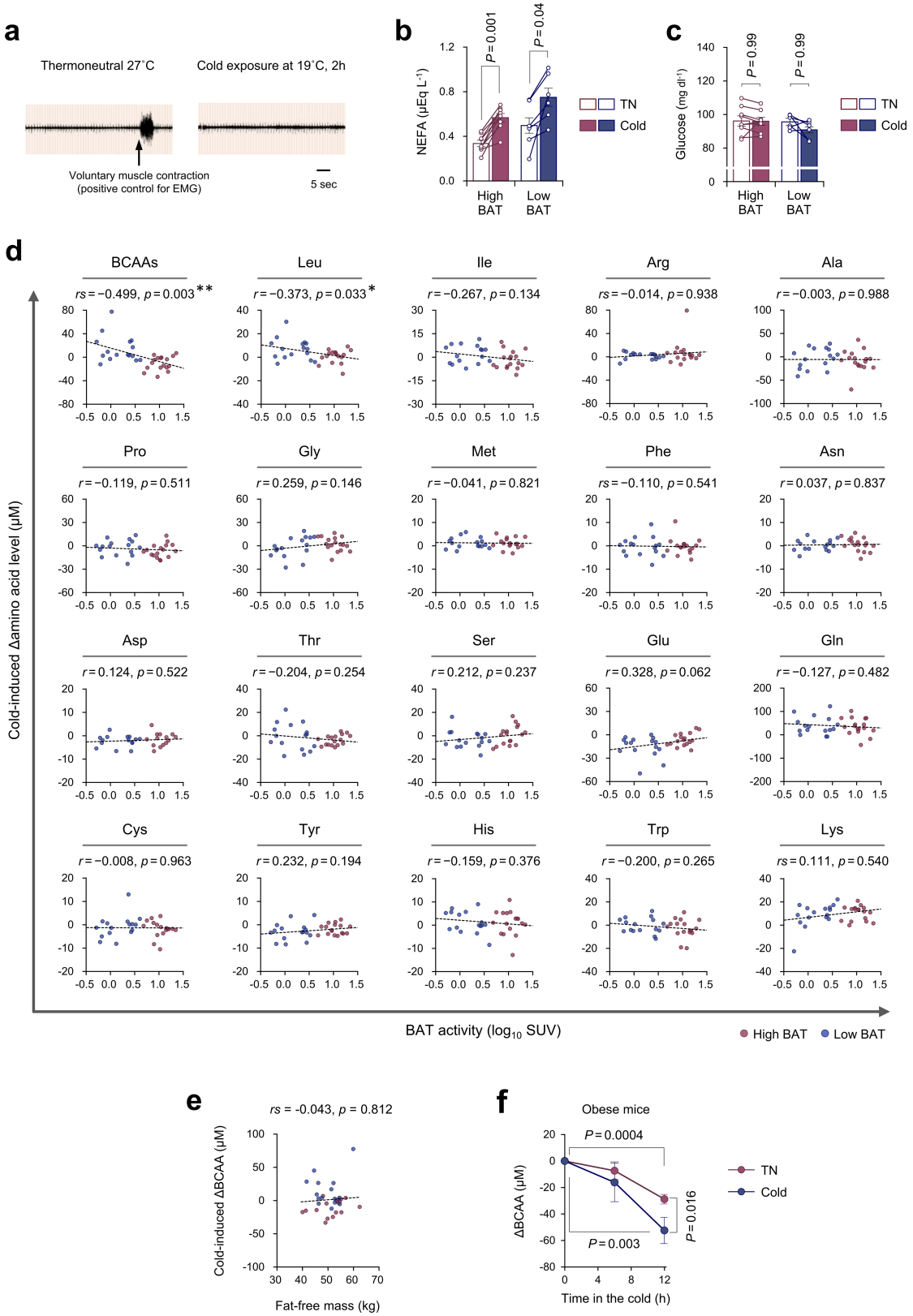

Extended Data Fig. 1 | Cold-induced changes in circulating metabolites in mice and humans. a, Representative EMG in adult humans at 27 °C and following cold exposure at 19 °C for 2 h. Voluntary muscle contraction as a positive control of EMG recording. **b**, **c**, Serum non-esterified fatty acids (NEFA) (**b**) and blood glucose (**c**) levels in high- ($n = 9$) and low-BAT subjects ($n = 6$) at thermoneutral 27 °C (TN) and following cold exposure at 19 °C. **d**, Correlation between BAT activity (SUV, $\log_{10}$) and cold-induced changes in serum amino acid levels of high- (red dots) and low-BAT subjects (blue dots). $n = 33$ per group (all amino acids) except $n = 29$ (Asp). **e**, Correlation between fat-free mass (kg) and changes in serum total BCAAs in **d**. $n = 33$. **f**, Changes in plasma BCAA levels at thermoneutral (30 °C) or cold exposure (15 °C) in diet-induced obese mice. $n = 8$ (TN), $n = 7$ (cold). **b**–**f**, Biologically independent samples. Data are mean ± s.e.m.; two-sided P values by paired t-test (**b**, **c**) or two-way repeated-measures ANOVA followed by post hoc paired or unpaired t-tests with Bonferroni's correction (**f**). Pearson's (r) or Spearman's rank correlation coefficient (rs) was calculated, as appropriate (**d**, **e**).

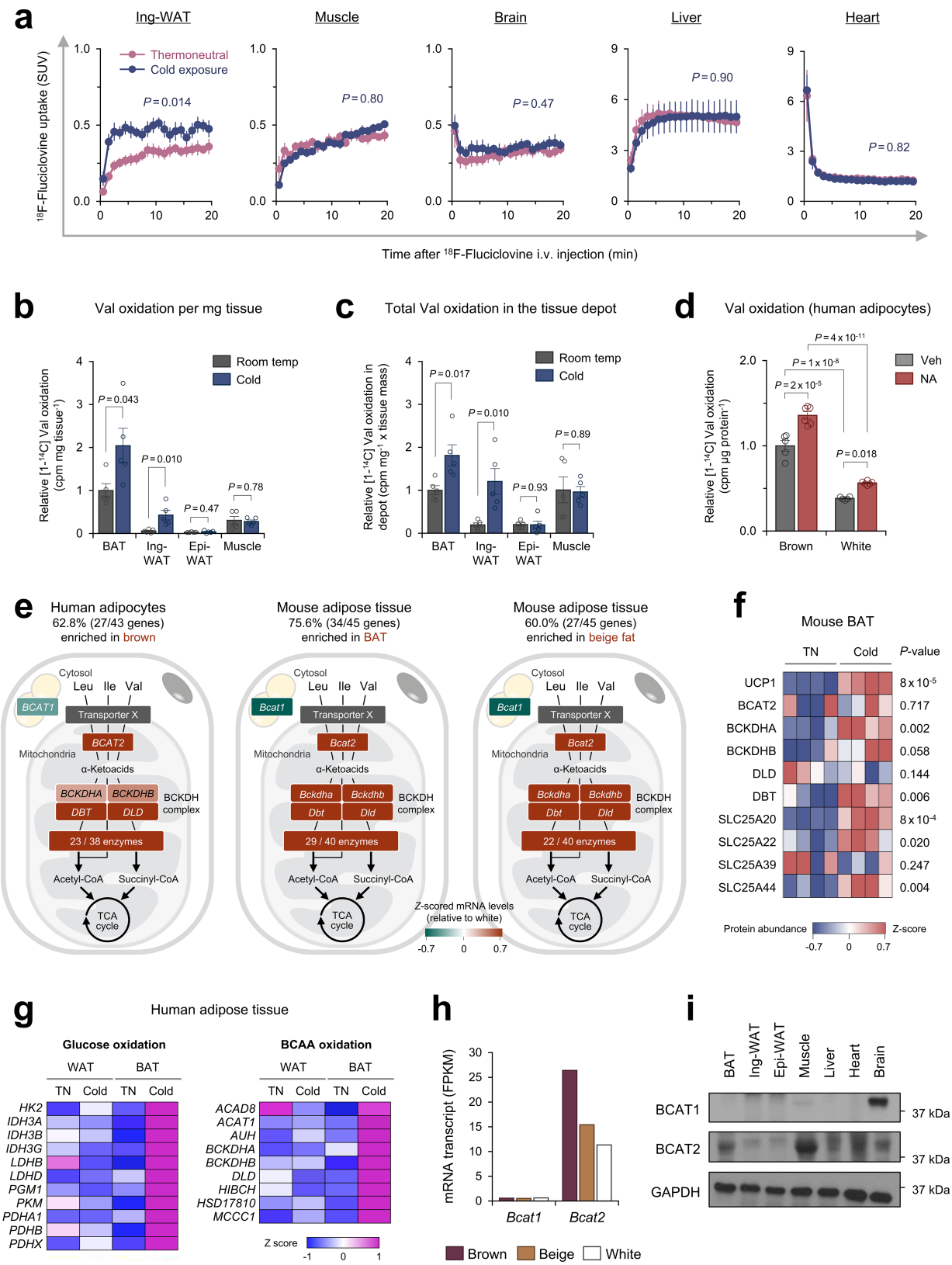

Extended Data Fig. 2 | See next page for caption.

Extended Data Fig. 2 | The BCAA catabolic pathway in human and mouse adipose tissues. a, ^{18}F-Fluciclovine-uptake into indicated organs determined by dynamic PET scanning. $n = 5$ per group. **b**, Val oxidation (per mg tissue) in indicated tissues of mice acclimatized to 23 °C or 12 °C for one week. $n = 5$ per group. **c**, Total Val oxidation in (**b**). Total Val oxidation was calculated by multiplying Val oxidation per mg tissue (cpm per mg tissue) and tissue mass of the depot (mg). **d**, Val oxidation normalized to total protein (μg) in human brown adipocytes and white adipocytes following 2-h treatment with noradrenaline or vehicle. $n = 5$ (Veh), $n = 6$ (noradrenaline). **e**, Expression profile of BCAA catabolic enzymes enriched in brown and beige fat relative to white fat of humans (left) and mouse (middle, right). Data were obtained from a previous RNA-seq dataset in humans[15] and a microarray dataset in mice[17]. The profiles were mapped onto the KEGG BCAA catabolic pathway. The number of brown and beige-enriched enzymes among total BCAA catabolic enzymes is shown. $n = 3$ per group. **f**, Proteomic profile of indicated enzymes in the BCAA oxidation pathway and mitochondrial carriers (SLC25A families) in interscapular BAT of mice at thermoneutrality (29 °C) or 5 °C for 3 weeks[16]. $n = 4$ per group. **g**, Transcriptional profile of indicated genes in the glucose oxidation pathway (left) and the BCAA oxidation pathway (right) in the supraclavicular BAT and abdominal WAT from the identical subject under a thermoneutral condition (27 °C) and after cold exposure at 19 °C (ref. [5]). The colour scale represents *Z*-scored FPKM (fragments per kilobase of exon per million fragments mapped). **h**, mRNA expression level (FPKM) of *Bcat1* and *Bcat2* in differentiated brown adipocytes, beige adipocytes and white adipocytes. The transcriptome data are from a previous RNA-seq dataset[15]. **I**, Immunoblotting of BCAT1 and BCAT2 in indicated tissues of mice kept at ambient temperature. GAPDH as a loading control. Representative result from two independent experiments. Gel source data are in Supplementary Fig. 1. **a**–**h**, biologically independent samples. Data are mean ± s.e.m.; two-sided *P* values by unpaired Student's *t*-test (**b**, **c**, **f**), two-way repeated measures ANOVA (**a**), or two-way factorial ANOVA followed by Tukey's post hoc test (**d**).

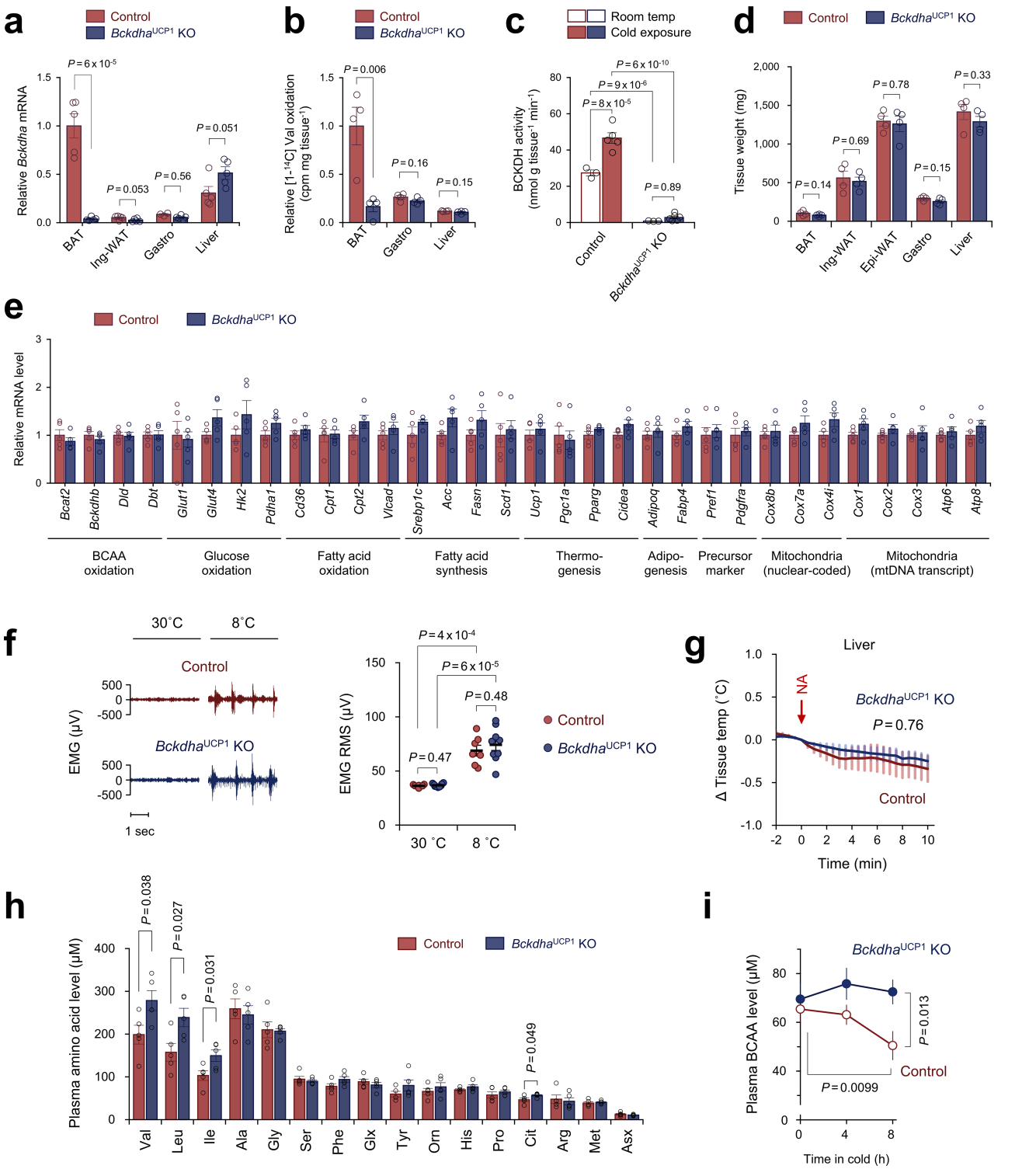

Extended Data Fig. 3 | Characterization of BAT-specific *Bckdha*-KO mice. a, mRNA expression of *Bckdha* in BAT of *Bckdha*^{UCP1}-KO and littermate control mice. $n = 5$ per group for all groups except $n = 3$ for control-gastrocnemius. **b**, Val oxidation normalized to tissue weight (in mg) in indicated tissues of mice in **a**. $n = 4$ per group. **c**, Enzymatic activity of BCKDH complex (KIV oxidation) in BAT of control and *Bckdha*^{UCP1}-KO mice acclimatized to 23 °C ($n = 3$ per group) or 12 °C (control $n = 5$, KO $n = 6$) for one week. **d**, Tissue weights of mice in (**a**) on a normal chow at ambient temperature. $n = 4$ per group. **e**, mRNA expression of indicated genes in BAT of mice in **a**. $n = 5$ per group. **f**, EMG of muscle shivering in control ($n = 7$) and *Bckdha*^{UCP1}-KO mice ($n = 9$) at 30 °C or 8 °C. The right graph shows quantitative root mean square (RMS) of EMG. **g**, Liver temperature of control and *Bckdha*^{UCP1}-KO mice following noradrenaline treatment. $n = 4$ per group. **h**, Plasma amino acid levels after 3 h BCAA oral gavage. $n = 5$ per group. **i**, Plasma BCAA concentration of control ($n = 7$) and *Bckdha*^{UCP1}-KO mice ($n = 9$) following cold exposure at 8 °C. **a**–**i**, Biologically independent samples. Data are mean ± s.e.m.; two-sided *P* values by unpaired Student's *t*-test (**a**, **b**, **d**, **e**, **h**), two-way factorial ANOVA followed by Tukey's post hoc test (**c**), or two-way repeated measures ANOVA (**f**, **g**, **i**) followed by post hoc paired or unpaired *t*-tests with Bonferroni's correction (**f**, **i**).

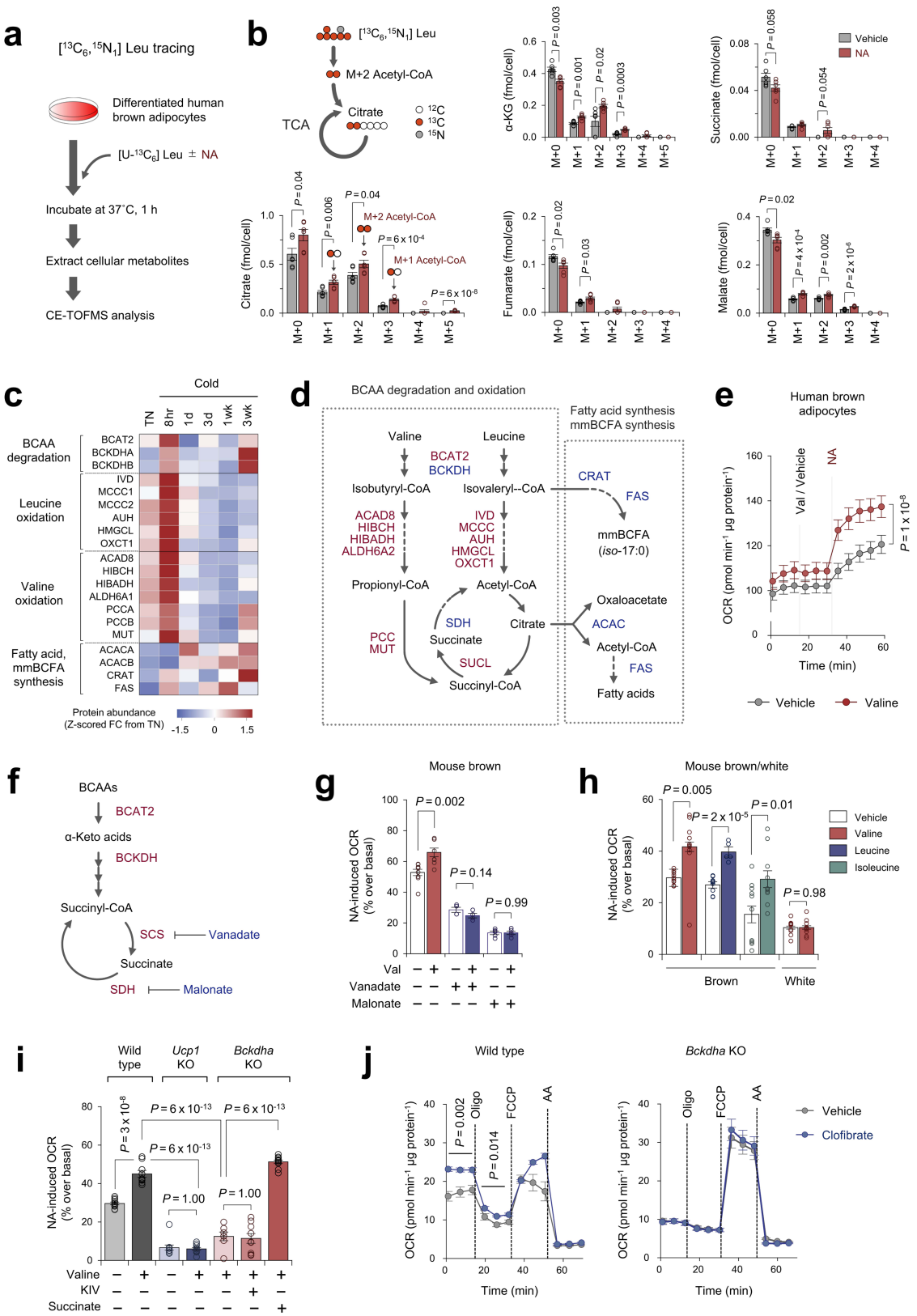

Extended Data Fig. 4 | See next page for caption.

Extended Data Fig. 4 | The effect of noradrenaline on BCAA metabolism in brown adipocytes. a, Scheme of the metabolic tracer experiment in human brown adipocytes. Cells were treated with vehicle or noradrenaline for 1 h in the presence of [$^{13}C_6$, $^{15}N_1$]Leu. **b**, Isotopologue distributions of TCA intermediates from [$^{13}C_6$, $^{15}N_1$]Leu in **a**. $n = 6$ per group. **c**, Protein expression of indicated BCAA catabolic enzymes at indicated time points of cold acclimatization. The expression profile is analysed in the proteomics dataset[16]. $n = 4$ (TN, cold 3 weeks), $n = 3$ (cold 8 h, 1 day, 3 days, 1 week). **d**, The BCAA catabolic pathway that indicates Val and Leu catabolic enzymes. Enzymes whose protein expression was transiently upregulated by acute cold exposure were highlighted in red on the basis of the results in **c**. Enzymes whose protein expression was gradually upregulated following chronic cold adaptation are highlighted in blue. **e**, OCR normalized to total protein (in μg) in human brown adipocytes. Differentiated adipocytes in the BCAA-free medium were supplemented with Val or vehicle, and subsequently stimulated with noradrenaline. $n = 10$ per group. **f**, Schematics of the mitochondrial Val catabolic pathway. Vanadate and malonate inhibit succinyl coenzyme A synthetase and succinate dehydrogenase, respectively. **g**, Noradrenaline-induced OCR in the presence and absence of Val in mouse brown adipocytes. Following pretreatment with vanadate (50 μM) or malonate (5 mM), differentiated cells in the BCAA-free medium were supplemented with Val or vehicle, and subsequently treated with noradrenaline. $n = 9$ (vehicle), $n = 8$ (Val), $n = 4$ (vehicle + vanadate, Val + vanadate), $n = 5$ (vehicle + malonate, Val + malonate). **h**, Noradrenaline-induced OCR in the presence and absence of BCAAs in mouse brown and white adipocytes. Differentiated cells were supplemented with indicated amino acids, and subsequently treated with 1 μM noradrenaline. Brown adipocytes: $n = 10$ (Val−, Val+, Ile+), 9 (Leu−), 5 (Leu+) and 11 (Ile−). White adipocytes: $n = 9$ (Val−) and 10 (Val+). **i**, Noradrenaline-induced OCR in the presence and absence of Val in wild-type, *Ucp1*-KO and *Bckdha*-KO brown adipocytes. *Bckdha*-KO brown adipocytes were treated with 2 mM KIV, 10 mM succinate or vehicle before noradrenaline stimulation. Wild type: $n = 10$ (Val−) and 9 (Val+). *Ucp1*-KO: $n = 10$ (Val−, Val+). *Bckdha* KO: $n = 7$ (Val+), 9 (Val+; KIV+) and 10 (Val+; succinate+). **j**, OCR normalized to total protein (μM) in wild-type (left) and *Bcdkha*-KO brown adipocytes (right). Differentiated adipocytes were pretreated with BCAT2 activator, clofibrate (300 μM), or vehicle. Following measurement of basal OCR, cells were treated with oligomycin (5 μM), FCCP (5 μM), and antimycin A (AA, 5 μM). Wild type: $n = 5$ per group. *Bckdha* KO: $n = 7$ per group. **b**, **c**, **e**, **g–j**, Biologically independent samples. Data are mean ± s.e.m.; two-sided *P* values by unpaired Student's *t*-test (**b**, **g**, **h**), one-way factorial ANOVA followed by Tukey's post hoc test (**i**) or two-way repeated measures ANOVA (**e**, **j**).

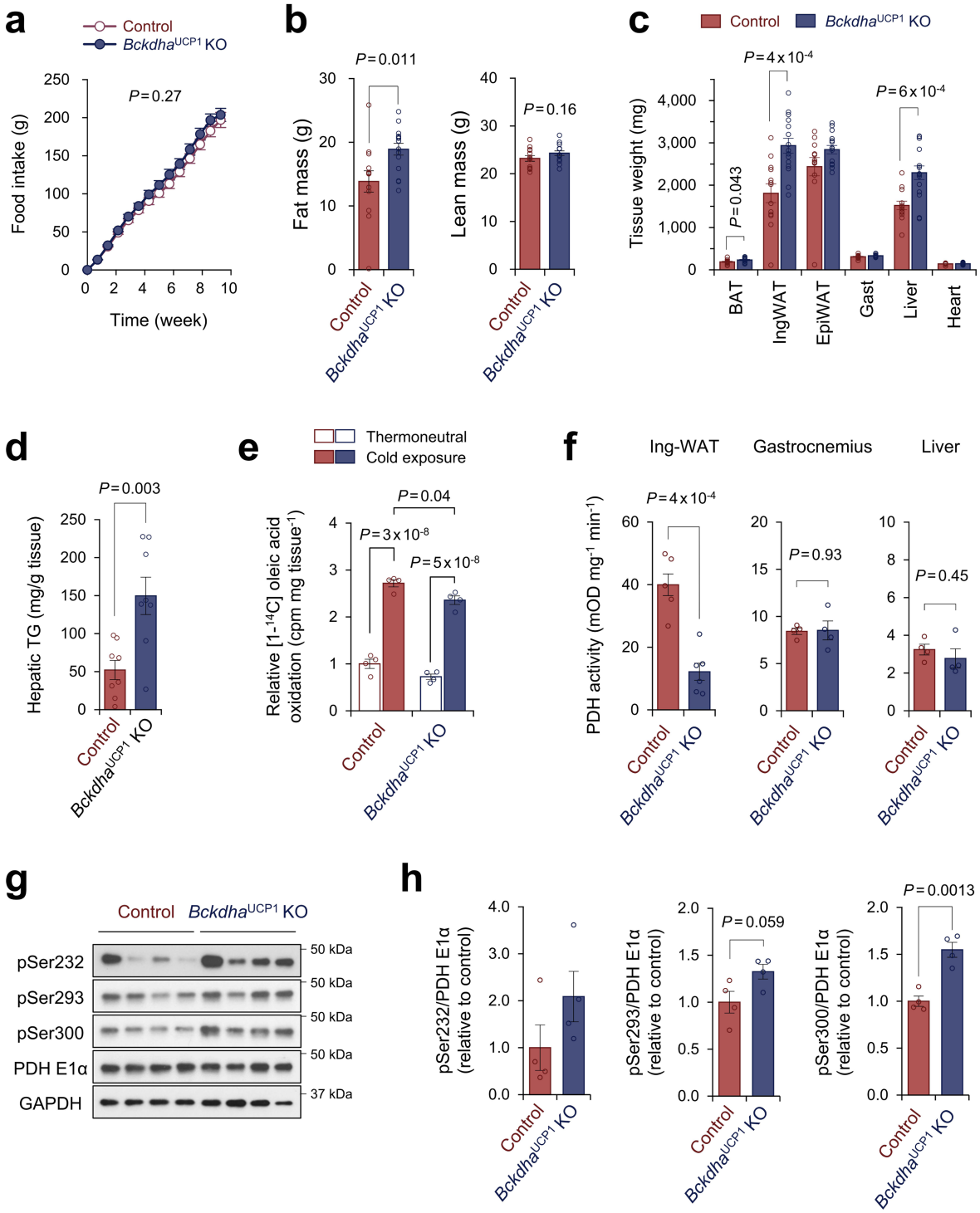

Extended Data Fig. 5 | Metabolic characterization of *Bckdha*^{UCP1}-KO mice. **a**, Cumulative food intake of *Bckdha*^{UCP1}-KO mice ($n = 15$) and littermate controls ($n = 13$) on high-fat diet. **b**, Fat mass and lean mass of mice in **a** at 10 weeks of high-fat diet. **c**, Tissue weights of mice in **a**. **d**, Triglyceride (TG) content in the liver of mice in **a**. $n = 8$ per group. **e**, Oleic acid oxidation normalized to tissue mass (mg) in the interscapular BAT of mice acclimatized to thermoneutral 30 °C or cold exposure at 12 °C. $n = 4$ per group. **f**, PDH activity in the inguinal WAT, gastrocnemius muscle and liver of *Bckdha*^{UCP1}-KO mice and littermate controls that were exposed to cold at 12 °C for 1 week. Inguinal WAT (Ing-WAT): $n = 5$ (control) and 6 (*Bckdha*^{UCP1}-KO). Gastrocnemius, liver: $n = 4$ per group. **g**, Immunoblotting for PDH-E1α(pSer232), PDH-E1α(pSer293), PDH-E1α(pSer300), and total PDH-E1α in the BAT of the control and *Bckdha*^{UCP1}-KO mice. GAPDH as a loading control. $n = 4$ per group. Uncropped immunoblot images of are available in Supplementary Fig. 1. **h**, Quantification of phosphorylated PDH-E1α normalized to total PDH-E1α protein level in **g**. **a**–**h**, Biologically independent samples. Data are mean ± s.e.m.; two-sided *P* values by unpaired Student's *t*-test (**b**-**d**, **f**, **h**), two-way repeated measures ANOVA (**a**) or two-way factorial ANOVA followed by Tukey's post hoc test (**e**).

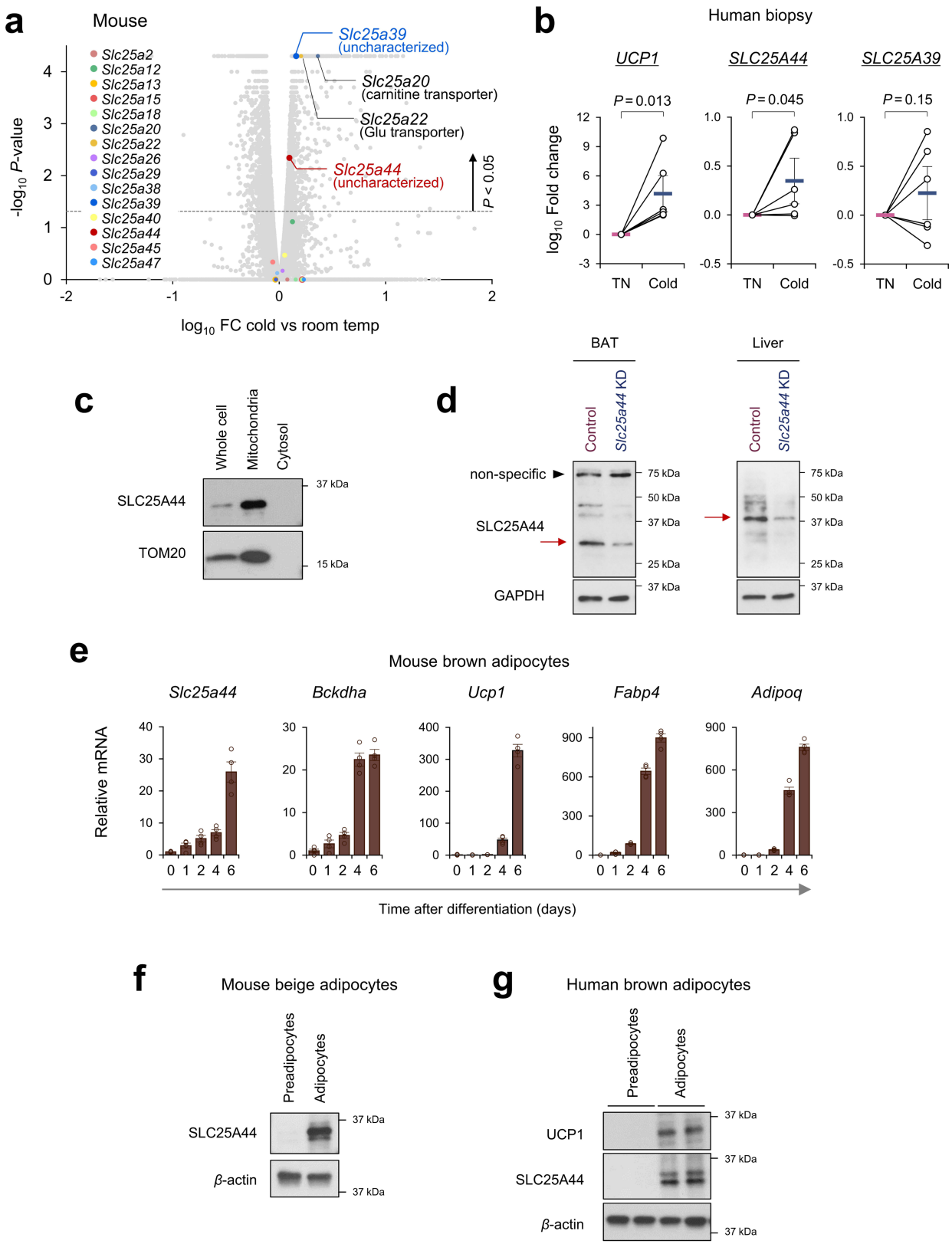

Extended Data Fig. 6 | See next page for caption.

Extended Data Fig. 6 | Characterization of SLC25A44 in thermogenic adipocytes. a, Expression profile of Slc25a family members in the inguinal WAT of mice acclimatized to 23 °C or 12 °C for 1 week. $n = 3$ per group. **b**, mRNA expression of *UCP1*, *SLC25A44* and *SLC25A39* normalized to *TBP* levels in the supraclavicular BAT from the same individuals (six pairs) at thermoneutrality (27 °C) and cold temperature (19 °C). **c**, Mitochondrial localization of SLC25A44 protein in differentiated mouse beige adipocytes. TOM20 was used as a mitochondrial marker. **d**, Immunoblotting for SLC25A44 in BAT and liver of control and *Slc25a44*-KD mice. GAPDH was used as a loading control. Red arrows indicate specific bands whose intensities were decreased in *Slc25a44*-KD mice. **e**, mRNA expression of *Slc25a44* and indicated genes normalized to levels of *36B4* (also known as *Rplp0*) during mouse brown adipogenesis. $n = 4$ per group. **f**, Protein expression of SLC25A44 in mouse beige preadipocytes and differentiated adipocytes. β-actin was used as a loading control. **g**, Protein expression of UCP1 and SLC25A44 in immortalized human brown preadipocytes and differentiated adipocytes. β-actin was used as a loading control. **a**, **b**, **e**, Biologically independent samples. Data are mean ± s.e.m.; one-sided *P* values by paired *t*-test (**b**) and two-sided *P* values by unpaired Student's *t*-test (**a**). **c**, **d**, **f**, **g**, Representative results from two independent experiments. Uncropped images are available in Supplementary Fig. 1.

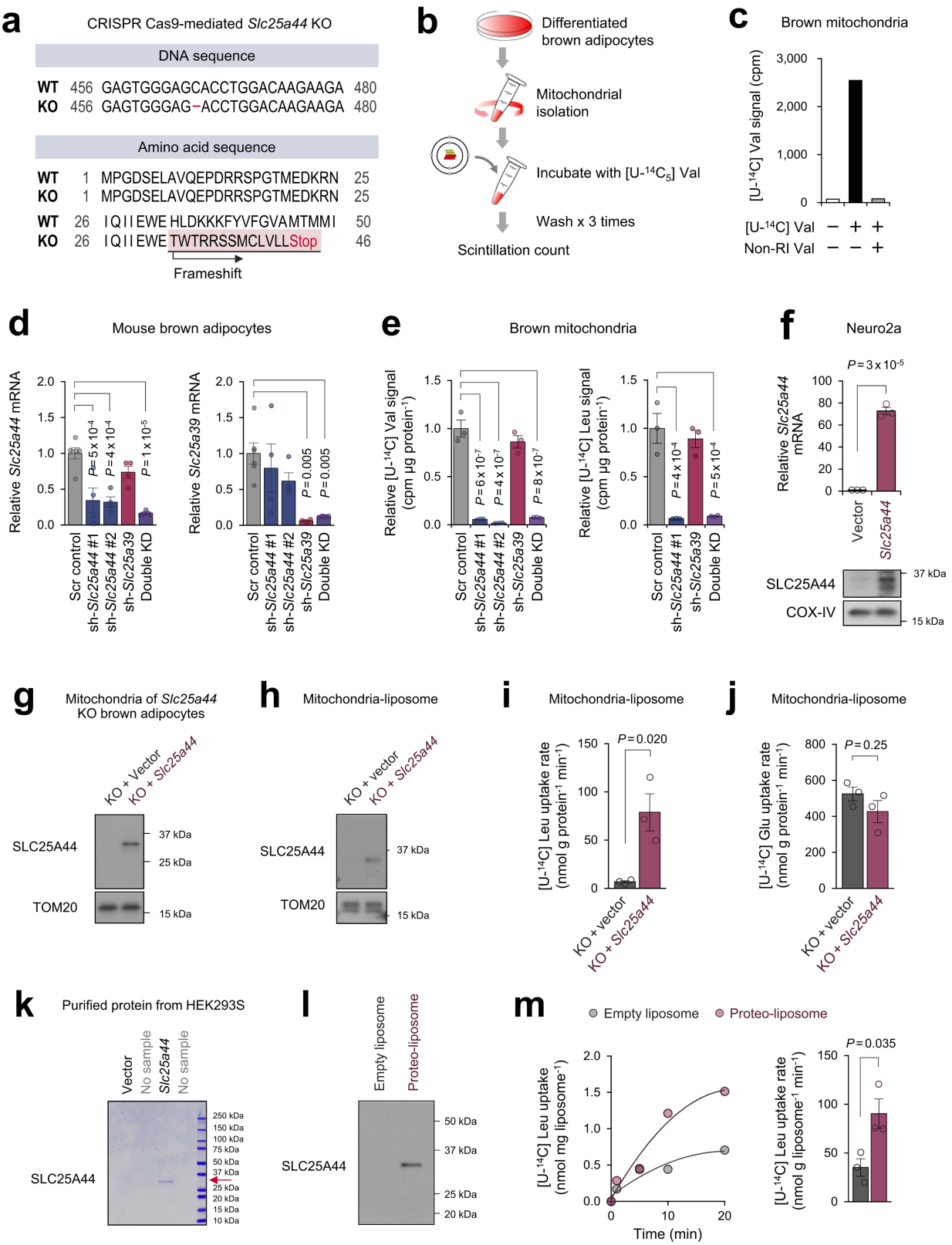

Extended Data Fig. 7 | See next page for caption.

Extended Data Fig. 7 | Biochemical characterization of SLC25A44. **a**, Genomic *Slc25a44* sequence of *Slc25a44*-KO brown cell line (upper panel). Predicted amino acid sequence of SLC25A44 is shown in lower panel. Homozygous mutation in the *Slc25a44* gene by CRISPR-Cas9 results in a premature stop codon in KO cells. **b**, Scheme of mitochondrial BCAA uptake assay. Isolated mitochondria from differentiated brown adipocytes were incubated with [U-$^{14}C_5$]Val. Mitochondrial uptake was quantified by a scintillation counter. **c**, Validation of mitochondrial Val uptake assay in differentiated brown adipocytes. Note that addition of excess non-labelled Val (20 mM) abolished [U-$^{14}C_5$]Val uptake into the mitochondria. **d**, mRNA expression of *Slc25a44* and *Slc25a39* in differentiated mouse brown adipocytes expressing a scrambled control shRNA (Scr, $n = 6$) and shRNAs targeting *Slc25a44* (shRNA #1, #2, $n = 4$ per group), *Slc25a39* ($n = 4$) or both *Slc25a44* shRNA #1 and *Slc25a39* shRNA (double knockdown, $n = 5$). **e**, Mitochondrial uptake of [U-$^{14}C_5$]Val (left) and [U-$^{14}C_6$]Leu (right) in brown adipocytes in (**d**). $n = 3$ per group. **f**, mRNA and protein expression of *Slc25a44* in mitochondria of Neuro2a cells expressing an empty vector or *Slc25a44*. COX-IV was used as a loading control. $n = 3$ per group. **g**, Immunoblotting for SLC25A44 in the isolated mitochondria from differentiated *Slc25a44*-KO brown adipocytes expressing an empty vector or *Slc25a44*. TOM20 was used as a loading control. **h**, Immunoblotting of SLC25A44 in the mitochondria-fused liposome. Mitochondrial membrane isolated from *Slc25a44*-KO brown adipocytes expressing an empty vector or *Slc25a44* was fused with liposome. TOM20 was used as a loading control. **i**, [U-$^{14}C_6$]Leu uptake rate in the liposome in **h**. $n = 3$ per group. **j**, [U-$^{14}C_5$]Glu uptake rate in the liposome in **h**. $n = 3$ per group. **k**, Coomassie blue staining of purified SLC25A44 protein from HEK293S cells overexpressing *Slc25a44*. **l**, Immunoblotting of SLC25A44 in liposomes reconstituted with purified SLC25A44 (proteoliposome) and liposomes reconstituted without SLC25A44 (empty liposome). **m**, Left, [U-$^{14}C_6$]Leu transport into proteoliposomes in **l**. Right, Leu uptake rate. $n = 3$ per group. **d**–**f**, Biologically independent samples. **i**, **j**, **m**, Technically independent samples. **f**–**m**, Representative result from two independent experiments. Data are mean ± s.e.m.; two-sided *P* values by unpaired Student's *t*-test (**f**, **i**, **j**, **m**) or one-way ANOVA followed by Tukey's post hoc test (**d**, **e**). **f**–**h**, **k**, **l**, Uncropped images are available in Supplementary Fig. 1.

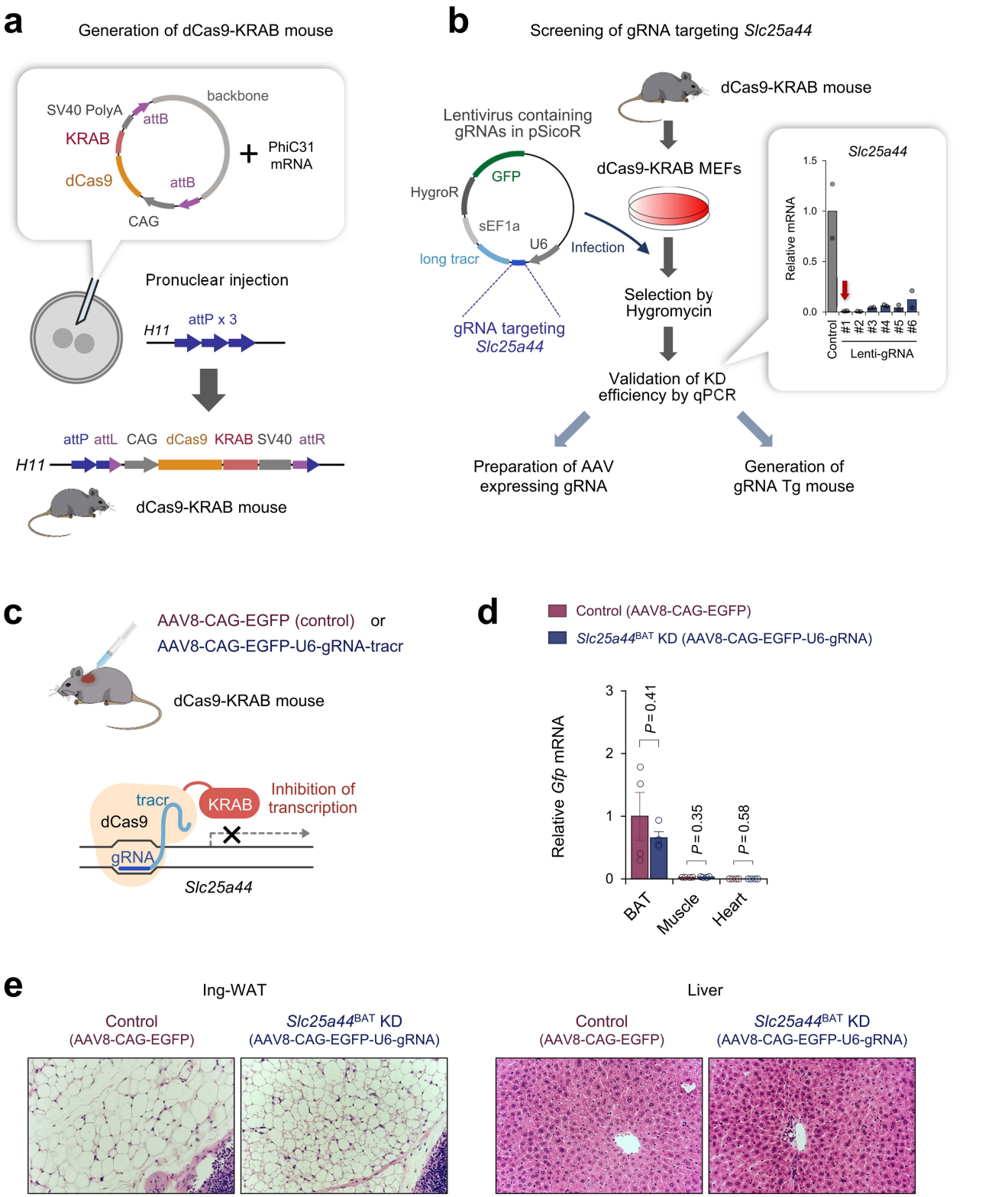

Extended Data Fig. 8 | Generation of *Slc25a44*^{BAT}-KD mice. a, DNA constructs used in the generation of dCas9-KRAB mice. The dCas9-KRAB construct was inserted into the *Hipp11* (H11) gene locus by the site-specific PhiC31 integrase. **b**, Experimental procedure of gRNA screening. MEFs from dCas9-KRAB mice were used to identify gRNA that effectively deplete *Slc25a44*. Graph shows *Slc25a44*-knockdown efficiency for six independent gRNAs in the dCas9-KRAB-derived MEFs ($n = 2$ per group). gRNA-*Slc25a44* #1 (indicated by a red arrow) was used for generation of gRNA Tg mouse. **c**, Schematics of BAT-specific *Slc25a44*-KD mice (*Slc25a44*^{BAT}-KD) by using the dCas9-KRAB system. AAV8-CAG-eGFP-U6-gRNA-tracr targeting *Slc25a44* was injected into the interscapular BAT of mice expressing dCas9-KRAB on the H11 locus (dCas9-KRAB mouse). AAV8-CAG-eGFP without gRNA was used as a control. **d**, mRNA expression of *Gfp* normalized to *36B4* in the indicated tissues of dCas9-KRAB mice in **c**. $n = 4$ per group. **e**, H&E staining of inguinal WAT and liver of control and *Slc25a44*^{BAT}-KD mice. **b**, **d**, biologically independent samples. Data are mean ± s.e.m.; two-sided *P* values by unpaired Student's *t*-test (**d**).

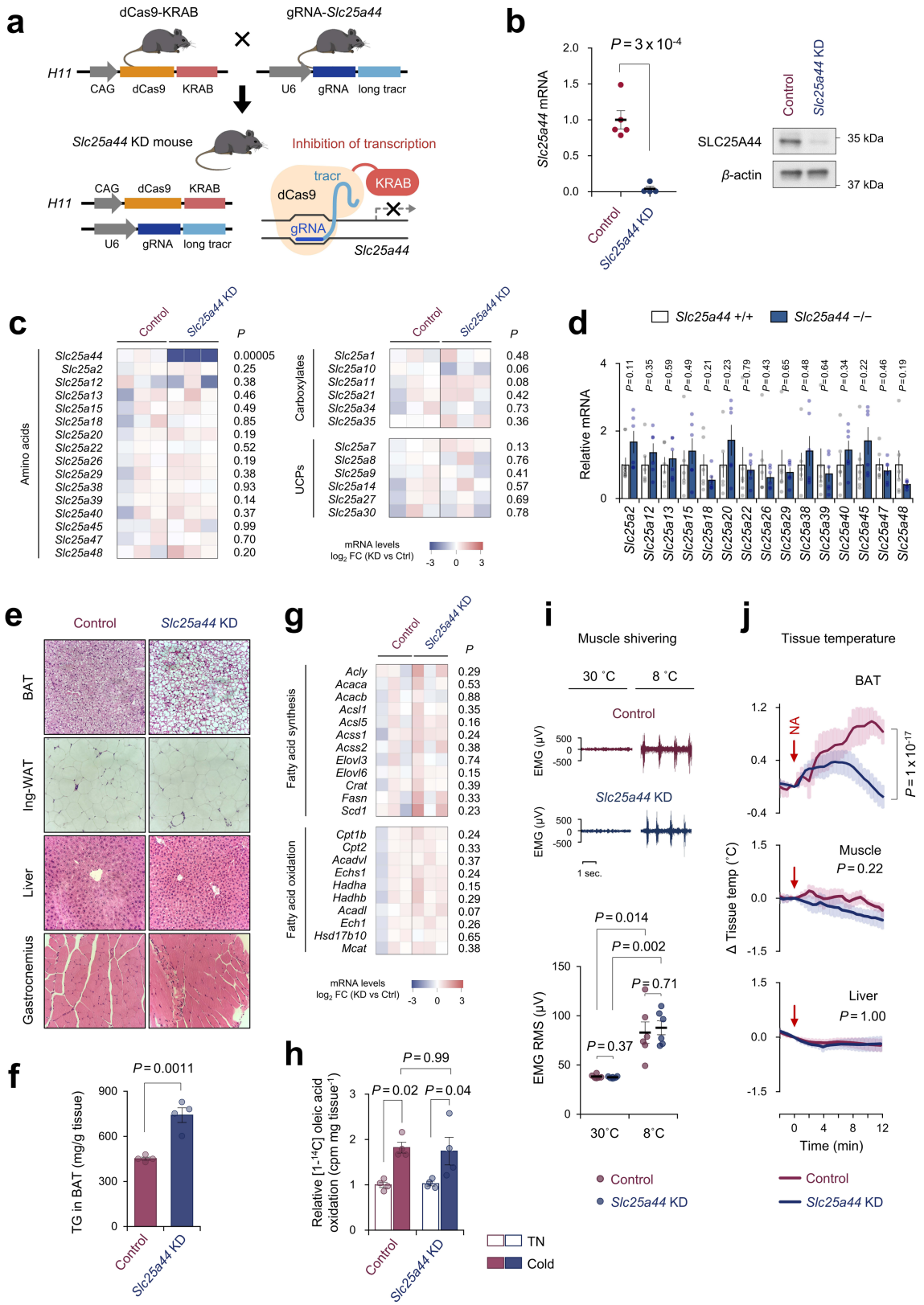

Extended Data Fig. 9 | See next page for caption.

Extended Data Fig. 9 | Characterization of *Slc25a44*-KD mice. **a**, Generation of *Slc25a44*-KD mice by the dCas9-KRAB system. The dCas9-KRAB mouse was crossed with transgenic mouse expressing gRNA targeting *Slc25a44* to generate SLC25A44 deficient mice. **b**, *Slc25a44* mRNA expression normalized to *36B4* levels and protein expression in the BAT of mice in **a**. β-actin was used as a loading control. $n = 5$ (control) and 4 (*Slc25a44*-KD). **c**, Expression profile of Slc25a family members in BAT in **a** by RNA-seq analysis. The colour scale shows $\log_2$-transformed fold change in TPM (*Slc25a44*-KD versus control). $n = 3$ per group. **d**, mRNA expression of *Slc25a* families normalized to *36B4* levels in *Slc25a44*-KO and control brown adipocytes. $n = 6$ per group. **e**, H&E staining of BAT, inguinal WAT, liver and gastrocnemius muscle from mice in **a**. **f**, Triglyceride content in the interscapular BAT of *Slc25a44*-KD and control mice. $n = 4$ per group. **g**, Expression profile of fatty acid synthesis- and oxidation-related genes in BAT of mice in **a** by RNA-seq analysis. The colour scale shows $\log_2$-transformed fold change in TPM (*Slc25a44*-KD versus control). $n = 3$ per group. **h**, Oleic acid oxidation normalized to tissue mass (mg) in BAT of *Slc25a44*-KD and control mice acclimatized to thermoneutral 30 °C or cold temperature (12 °C) for one week. $n = 4$ per group. **i**, EMG measurement of muscle shivering in control mice and *Slc25a44*-KD mice at 30 °C or 8 °C. The lower graph shows the RMS of the EMG. $n = 6$ per group. **j**, Tissue temperature in indicated tissues of control and *Slc25a44*-KD mice following noradrenaline treatment (indicated by red arrows). $n = 4$ per group. **b**–**d**, **f**–**j**, Biologically independent samples. Data are mean ± s.e.m.; two-sided *P* values by unpaired Student's *t*-test (**b**–**d**, **f**, **g**), two-way factorial ANOVA followed by Tukey's post hoc test (**h**), or two-way repeated measures ANOVA (**i**, **j**) followed by post hoc paired or unpaired *t*-test with Bonferroni's correction (**i**). **b**, **e**, Representative results from two independent experiments. Uncropped immunoblot images are available in Supplementary Fig. 1.

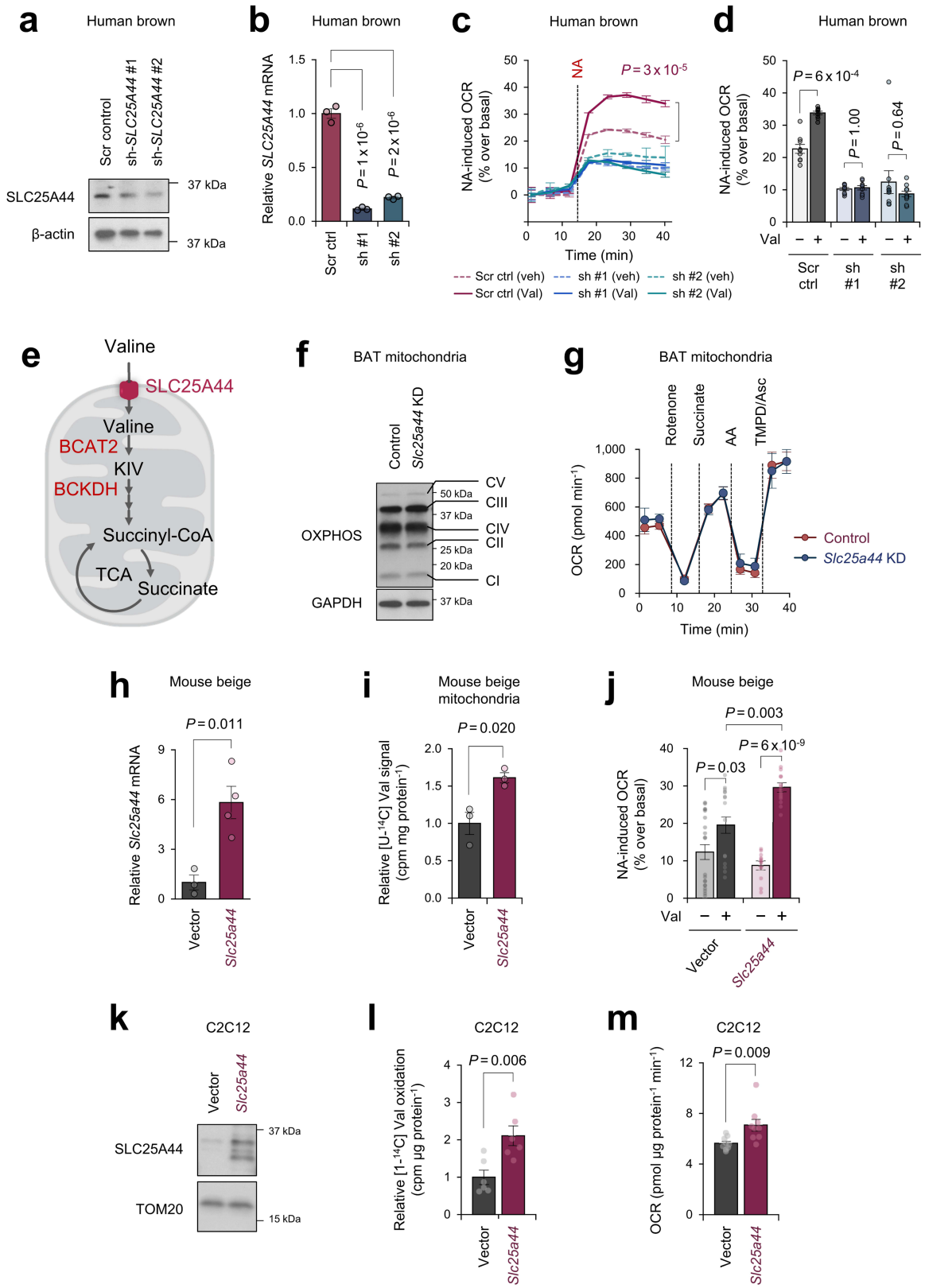

Extended Data Fig. 10 | See next page for caption.

Extended Data Fig. 10 | The cell-autonomous role of SLC25A44 in brown adipocytes. a, Immunoblotting of SLC25A44 in human brown adipocytes expressing a scrambled control shRNA (Scr) and shRNAs targeting *SLC25A44* (#1, #2). β-actin as a loading control. **b**, mRNA expression of *SLC25A44* normalized to *TBP* levels in **a**. $n = 3$ per group. **c**, Noradrenaline-induced OCR normalized to total protein (μg) in the presence and absence of Val supplementation in **a**. Differentiated human brown adipocytes in the BCAA-free medium were supplemented with Val or vehicle, and subsequently treated with noradrenaline. $n = 9$ per group (Scr control, sh-*Slc25a44* #1), $n = 10$ per group (sh-*Slc25a44* #2). **d**, Mean noradrenaline-induced OCR in **c**. **e**, Illustration of Val metabolism in the mitochondria. **f**, Immunoblotting of mitochondrial proteins (as indicated) in the interscapular BAT of control and *Slc25a44*-KD mice. GAPDH as a loading control. **g**, ETC activity of BAT mitochondria. Isolated mitochondria from BAT of control mice and *Slc25a44*-KD mice were treated with rotenone (2 μM), succinate (10 mM), antimycin A (5 μM) and TMPD (100 μM) with ascorbate (Asc, 10mM). $n = 5$ per group. **h**, mRNA expression of *Slc25a44* normalized to *36B4* in mouse beige adipocytes expressing an empty vector ($n = 3$) or *Slc25a44* ($n = 4$). **i**, Mitochondrial Val uptake in beige adipocytes in **h**. $n = 3$ per group. **j**, Noradrenaline-induced OCR in **h**. Differentiated adipocytes in the BCAA-free medium were supplemented with Val or vehicle and subsequently stimulated with noradrenaline. Vector: $n = 20$ (vehicle) and 16 (Val). *Slc25a44*: $n = 13$ (vehicle) and 16 (Val). **k**, Immunoblotting of SLC25A44 in C2C12 myotubes expressing an empty vector or *Slc25a44*. β-actin as a loading control. **l**, Val oxidation normalized to total protein (μg) in C2C12 myotubes in **k**. $n = 6$ per group. **m**, OCR normalized to total protein (μg) in C2C12 myotubes in **k**. $n = 9$ per group. **b**–**d**, **g**–**j**, **l**, **m**, Biologically independent samples. Data are mean ± s.e.m.; two-sided *P* values by unpaired Student's *t*-test (**h**, **i**, **l**, **m**), one-way (**b**) or two-way (**d**, **j**) factorial ANOVA followed by Tukey's post hoc test, or two-way repeated measures ANOVA (**c**, **g**). **a**, **f**, **k**, Representative results from two independent experiments. Uncropped immunoblot images are available in Supplementary Fig. 1.

nature research

Corresponding author(s): Shingo Kajimura

Reporting Summary

Nature Research wishes to improve the reproducibility of the work that we publish. This form provides structure for consistency and transparency in reporting. For further information on Nature Research policies, see Authors & Referees and the Editorial Policy Checklist.

Statistical parameters

When statistical analyses are reported, confirm that the following items are present in the relevant location (e.g. figure legend, table legend, main text, or Methods section).

n/a	Confirmed	
☐	☒	The exact sample size (*n*) for each experimental group/condition, given as a discrete number and unit of measurement
☐	☒	An indication of whether measurements were taken from distinct samples or whether the same sample was measured repeatedly
☐	☒	The statistical test(s) used AND whether they are one- or two-sided *Only common tests should be described solely by name; describe more complex techniques in the Methods section.*
☒	☐	A description of all covariates tested
☐	☒	A description of any assumptions or corrections, such as tests of normality and adjustment for multiple comparisons
☐	☒	A full description of the statistics including central tendency (e.g. means) or other basic estimates (e.g. regression coefficient) AND variation (e.g. standard deviation) or associated estimates of uncertainty (e.g. confidence intervals)
☐	☒	For null hypothesis testing, the test statistic (e.g. *F*, *t*, *r*) with confidence intervals, effect sizes, degrees of freedom and *P* value noted *Give P values as exact values whenever suitable.*
☒	☐	For Bayesian analysis, information on the choice of priors and Markov chain Monte Carlo settings
☐	☒	For hierarchical and complex designs, identification of the appropriate level for tests and full reporting of outcomes
☐	☒	Estimates of effect sizes (e.g. Cohen's *d*, Pearson's *r*), indicating how they were calculated
☐	☒	Clearly defined error bars *State explicitly what error bars represent (e.g. SD, SE, CI)*

Our web collection on statistics for biologists may be useful.

Software and code

Policy information about availability of computer code

Data collection	PET-CT image: VOX-BASE workstation (for humans), Amide 1.0.4 (for mice) RNAseq analysis: Kallisto 0.44.0; TopHat version 2.0.8; Cuffdiff 2.1.1; Metascape; Ingenuity Pathway Analysis; tximport 1.10.0. QPCR: QuantStudio Real-time PCR system 1.2v Seahorse: Wave 2.4 EMG: LabChart 8
Data analysis	Microsoft office Excel 2016; SPSS statistics version 25.0; R package version 3.6.1

For manuscripts utilizing custom algorithms or software that are central to the research but not yet described in published literature, software must be made available to editors/reviewers upon request. We strongly encourage code deposition in a community repository (e.g. GitHub). See the Nature Research guidelines for submitting code & software for further information.

Data

Policy information about availability of data

All manuscripts must include a data availability statement. This statement should provide the following information, where applicable:

- Accession codes, unique identifiers, or web links for publicly available datasets
- A list of figures that have associated raw data
- A description of any restrictions on data availability

RNA-seq dataset generated in this study (Extended Data Fig.9c, 9g) is available at Array Express under the accession code E-MTAB-7987 (For reviewers accession code: Username: Reviewer_E-MTAB-7987, Password: ww5qvwph). Publicly available array datasets used in this study are GSE51080 (Extended Data Figure 2e), ArrayExpress E-MTAB-2602 (Extended Data Figure 2e), ArrayExpress MTAB-4031 (Extended Data Figure 2g), ArrayExpress E-MTAB-2624 (Extended Data Figure 2h). RNA-seq analysis in Extended Data Figure 6a is available in Source Data Extended Data Figure 6. Publicly available proteomics analysis dataset (Sustarsic EG et al. Cell Metab 28: 159-174, 2018 doi: 10.1016/j.cmet.2018.05.003) was used in Extended Data Figures 2f, 4c. 13C-labeled Leu metabolic tracing data is available in Supplementary Table 3.

Field-specific reporting

Please select the best fit for your research. If you are not sure, read the appropriate sections before making your selection.

☒ Life sciences ☐ Behavioural & social sciences ☐ Ecological, evolutionary & environmental sciences

For a reference copy of the document with all sections, see nature.com/authors/policies/ReportingSummary-flat.pdf

Life sciences study design

All studies must disclose on these points even when the disclosure is negative.

Sample size	The sample size was determined by the power analysis with α = 0.05 and power of 0.8, developed by Cohen (1988), and based on our experience with experimental models, anticipated biological variables, and previous literatures. Sample numbers were described in the Figure legends.
Data exclusions	No data were excluded in the study.
Replication	All the biological experiments were repeated, at least, twice and reproduced. RNA-sequencing and metabolomics were performed once but three independent samples were analyzed and further validated by alternative approaches, such as qRT-PCR. Western blotting data were confirmed by two or three independent samples.
Randomization	Mice were randomly assigned at the time of purchase or weaning to minimize any potential bias. This is described in the Method (animals).
Blinding	The metabolite analyses in human sera and mouse plasma, the [13C6, 15N1] leucine tracing in human brown adipocytes, the PET/CT examination using 18F-FDG (in humans) or 18F-Fluciclovine (in mice), and GTT/ITT in mice fed high fat diet were performed by the authors who were blinded to the experimental groups. RNA sequencing and library constructions were performed by technical staffs at the UCLA genome core who were blinded to the experimental groups. RNA sequencing alignment were performed by the authors who were blinded to the experimental groups. Blinding was not relevant to the other experiments in mice or cells because mice or cells had to be genotyped by PCR.

Reporting for specific materials, systems and methods

Materials & experimental systems

n/a	Involved in the study
☐	☒ Unique biological materials
☐	☒ Antibodies
☐	☒ Eukaryotic cell lines
☒	☐ Palaeontology
☐	☒ Animals and other organisms
☐	☒ Human research participants

Methods

n/a	Involved in the study
☒	☐ ChIP-seq
☒	☐ Flow cytometry
☒	☐ MRI-based neuroimaging

Unique biological materials

Policy information about availability of materials

Obtaining unique materials	All unique materials used are available from the authors upon reasonable request.

Antibodies

Antibodies used	Following antibodies were used in this study: - Anti-BCAT1 antibody, mouse monoclonal, 1:1000 (WB), OriGene (TA504360) - Anti-BCAT2 antibody, rabbit polyclonal, 1:1000 (WB), Cell Signaling Tech (9432) - Anti-BCKDHA antibody, mouse monoclonal, 1:2000 (WB), Santa Cruz (sc-271538) - Anti-COX-IV antibody, rabbit monoclonal, 1:2000 (WB), Cell Signaling Tech (4850) - Anti-Flag antibody, mouse monoclonal, 1:2000 (WB), Sigma (A8592) - Anti-GAPDH antibody, mouse monoclonal, 1:2000 (WB), Santa Cruz (sc-32233) - Anti-GFP antibody, chicken polyclonal, 1:200 (staining), Aves labs (GFP-1020) - Anti-chicken IgG, Alexa Fluor 488, Goat polyclonal, 1:500 (staining), Life Technologies (A11039) - Anti-OXPHOS antibody cocktail, mouse monoclonal, 1:2000 (WB), Abcam (ab110413) - Anti-PDH-E1α antibody, mouse monoclonal, 1:1000 (WB), Santa Cruz (sc-377092) - Anti-PDH-E1α (pSer232) antibody, rabbit polyclonal, 1:1000 (WB), Millipore (AP1063) - Anti-PDH-E1α (pSer293) antibody, rabbit monoclonal, 1:1000 (WB), Abcam (ab177461) - Anti-PDH-E1α (pSer300) antibody, rabbit polyclonal, 1:1000 (WB), Millipore (AP1064) - Anti-SLC25A44 antibody, rabbit polyclonal, 1:1000 (WB), GeneScript (custom order; it was generated by using amino acids (MEDKRNIQIIEWEHLDKKKC, MMQRKGEKMGRFQVC, and CKKLSLRPELVDSRH) as epitopes for immunization in rabbit. - Anti-TOM20 antibody, rabbit polyclonal, 1:2000 (WB), Proteintech (11802-1-AP) - Anti-UCP1 antibody, rabbit polyclonal, 1:2000 (WB), Abcam (ab-10983) - Anti-β-actin antibody, mouse monoclonal, 1:10000 (WB), Sigma (A3854)
Validation	All antibodies were validated for the application and species used in this study by their manufacturers and by the authors. Antibodies were validated based on the size of band in western blotting (molecular weight), specificity/selectivity assessed by using samples from knockout mouse/knockdown mouse/knockdown cells/over expression cells, and reproducibility of the results. - Anti-BCAT1 antibody: https://www.origene.com/catalog/antibodies/primary-antibodies/ta504360/bcat1-mouse-monoclonal-antibody-clone-id-oti3f5 - Anti-BCAT2 antibody: https://www.cellsignal.com/products/primary-antibodies/bcat2-antibody/9432 - Anti-BCKDHA antibody: https://www.scbt.com/scbt/product/bckde1a-antibody-h-5?productCanUrl=bckde1a-antibody - Anti-COX-IV antibody: https://www.cellsignal.com/products/primary-antibodies/cox-iv-3e11-rabbit-mab/4850 - Anti-Flag antibody: https://www.sigmaaldrich.com/catalog/product/sigma/a8592?lang=en&region=US - Anti-GAPDH antibody: https://www.scbt.com/scbt/product/gapdh-antibody-g-9?gclid=Cj0KCQjw9pDpBRCkARIsAOzRzivPevMxfm1PECD4RaBDNpW5UMHHdAHUYTrRaPub43MCQxsOIJzk_zEaAlJlEALw_wcB - Anti-GFP antibody: https://www.aveslabs.com/collections/epitope-tag-6xhis-beta-gal-actin-and-gfp-antibodies/products/green-fluorescent-protein-gfp-antibody - Anti-chicken IgG, Alexa Fluor 488: https://www.thermofisher.com/antibody/product/Goat-anti-Chicken-IgY-H-L-Secondary-Antibody-Polyclonal/A-11039 - Anti-OXPHOS antibody cocktail: https://www.abcam.com/total-oxphos-rodent-wb-antibody-cocktail-ab110413.html?gclid=Cj0KCQjw9pDpBRCkARIsAOzRziujlUlTLatVARYKCiIKIiq1Wu_-hEZ13i6E0vQrr9vd03Z4rUF5CowaAhY9EALw_wcB&productWallTab=ShowAll - Anti-PDH-E1α antibody: https://www.scbt.com/scbt/product/pdh-e1alpha-antibody-d-6 - Anti-PDH-E1α (pSer232) antibody: https://www.emdmillipore.com/US/en/product/PhosphoDetect-Anti-PDH-E1-pSer232-Rabbit-pAb,EMD_BIO-AP1063 - Anti-PDH-E1α (pSer293) antibody: https://www.abcam.com/pyruvate-dehydrogenase-e1-alpha-subunit-phospho-s293-antibody-epr12200-ab177461.html - Anti-PDH-E1α (pSer300) antibody: https://www.emdmillipore.com/US/en/product/PhosphoDetect-Anti-PDH-E1-pSer300-Rabbit-pAb,EMD_BIO-AP1064 - Anti-SLC25A44 antibody: Fig 4b; Ext Fig 6d; Ext Fig 7f-h,l; Ext Fig 9b; Ext Fig 10a,k. - Anti-TOM20 antibody: https://www.ptglab.com/products/TOM20-Antibody-11802-1-AP.htm - Anti-UCP1 antibody: https://www.abcam.com/ucp1-antibody-ab10983.html - Anti-β-actin antibody: https://www.sigmaaldrich.com/catalog/product/sigma/a3854?lang=en&region=US

Eukaryotic cell lines

Policy information about cell lines

Cell line source(s)	Preadipocytes were isolated from the interscapular BAT or the inguinal WAT of either wild type or Ucp1 -/- mice and immortalized by infecting retrovirus expressing SV-Large T antigen. Mouse embryonic fibroblasts (MEF) were isolated from dCas9-KRAB mice and immortalized by infecting retrovirus expressing SV-Large T antigen. Preadipocytes, isolated from either the supraclavicular BAT or subcutaneous WAT of healthy human participants, were immortalized, as reported previously (Shinoda et al. Nautre Medicine 2015).

	C2C12 (CRL-1772) and HEK293S (CRL-3022) were purchased from ATCC. Neuroblastoma cell line (Neuro2a) was purchased from Sigma-Aldrich (89121404).
Authentication	RNA-sequencing of the cell lines provide authentification.
Mycoplasma contamination	All the cell lines were routinely tested for mycoplasma infection and confirmed as negative for mycoplasma contamination.
Commonly misidentified lines (See ICLAC register)	No commonly misidentified cell line was used.

Animals and other organisms

Policy information about studies involving animals; ARRIVE guidelines recommended for reporting animal research

Laboratory animals	Mus musculus was used as an animal model. The strains were as followed: - C57BL/6J mice were obtained from the Jackson Laboratory. - Ucp1-Cre mice (Stock No. 024670) were obtained from the Jackson Laboratory. - Pparg flox mice (Stock No. 004584) were obtained from the Jackson Laboratory. - Bckdhatm1a(EUCOMM)Hmgu mice were obtained from EuMMCR and used for generation of Bckdha flox mice. - BAT-specific Bckdha-KO mice were generated by crossing Bckdha flox mouse and Ucp1-Cre mouse. - dCas9-KRAB mice were generated by a site-specific integrase-mediated approach (TARGATT system), in which a construct having dCas9-KRAB was integrated into H11 locus to express dCas9-KRAB ubiquitously. - Transgenic (Tg) mice of gRNA targeting Slc25a44 were generated by conventional transgenics. - Slc25a44 KD mice were generated by crossing dCas9-KRAB mouse and Slc25a44-gRNA mouse. Adult males and females aged 8-16 weeks were used for the experiments. Littermate controls with same sex were used. All the mice had free access to food and water, 12 hr light cycles, and were caged at 23 C.
Wild animals	This study did not involve wild animals
Field-collected samples	This study did not involve samples collected from the field.

Human research participants

Policy information about studies involving human research participants

Population characteristics	Thirty-three healthy young Japanese male volunteers participated in this study (23.4 ± 0.58 years old). BMI was within normal range (21.0 ± 0.30 kg/m2).
Recruitment	Volunteers were recruited by trial awareness-raising posters and consultant email-out. Potential selection biases were not detected/observed.